MOX-Report No. 103/2023

Robust Preconditioning of Mixed-Dimensional PDEs on 3d-1d domains coupled with Lagrange Multipliers

Dimola N.; Kuchta M.; Mardal K.A.; Zunino P.

MOX, Dipartimento di Matematica
Politecnico di Milano, Via Bonardi 9 - 20133 Milano (Italy)

mox-dmat@polimi.it https://mox.polimi.it

Robust Preconditioning of Mixed-Dimensional PDEs on $3d$-$1d$ domains coupled with Lagrange Multipliers

Nunzio Dimola, Miroslav Kuchta and Kent-Andre Mardal and Paolo Zunino

Abstract In the context of micro-circulation, the coexistence of two distinct length scales - the vascular radius and the tissue/organ scale - with a substantial difference in magnitude, poses significant challenges. To handle slender inclusions and simplify the geometry involved, a technique called *topological dimensionality reduction* is used, which suppresses the manifold dimensions associated with the smaller characteristic length. However, the algebraic structure of the resulting discretized system presents a challenge in constructing efficient solution algorithms. This chapter addresses this challenge by developing a robust preconditioner for the $3d$-$1d$ problem using the operator preconditioning technique. The robustness of the preconditioner is demonstrated with respect to the problem parameters, except for the vascular radius. The vascular radius, as demonstrated, plays a fundamental role in the mathematical well-posedness of the problem and the effectiveness of the preconditioner.

1 Introduction

The human cardiovascular system displays a diverse range of scales and characteristics, encompassing the major blood vessels, arterioles, and capillaries, with diameters ranging from several cm to a few μm. In particular, when examining the microcirculation, the challenge intensifies due to the substantial disparity in scale

Nunzio Dimola
MOX, Department of Mathematics, Politecnico di Milano, Italy, e-mail: nunzio.dimola@polimi.it

Miroslav Kuchta
Simula Research Laboratory, Oslo, Norway, e-mail: miroslav@simula.no

Kent-Andre Mardal
Department of Mathematics, University of Oslo, Norway,e-mail: kent-and@math.uio.no

Paolo Zunino
MOX, Department of Mathematics, Politecnico di Milano, Italy, e-mail: paolo.zunino@polimi.it

between the diameter of small vessels (μm) and the size of the corresponding system or organ they supply (dm). To deal with this disparity, intricate vascular networks that occupy space are needed, leading to complex geometric structures.

Due to the inherent complexities involved, simulating flow throughout the cardiovascular system is not practical or applicable. However, it is crucial to adopt a comprehensive approach that incorporates interactions between different system components by integrating models operating at various levels of detail. This approach is commonly referred to as *geometrical multi-scale* or *hybrid-dimensional modeling*.

Two types of hybrid-dimensional models can be considered: sequential and embedded. In an embedded multiscale model, components of varying levels of detail are integrated within the same domain. A prime example is the microcirculation, where a complex vascular network comprising arterioles, capillaries, and small veins exists within the biological tissue.

From a modeling point of view, such ideas have appeared in the last three decades (at least) for modeling wells in subsurface reservoirs in [39, 40] and for modeling microcirculation in [3, 13, 14, 45, 19]. A similar approach has recently been used to model soil/root interactions [22]. However, these application-driven seminal ideas were not followed by a systematic theory and rigorous mathematical analysis. At the same time, the models introduce additional mathematical complexity, in particular concerning the functional setting for the solution as it involves coupling PDEs on domains with high dimensionality gap. This mathematical challenge has recently attracted the attention of many researchers. The sequence of works by [10, 11, 12], followed by [31, 30, 27], has remedied the well-posedness by weakening the regularity assumptions that define a solution.

However, the mathematical understanding of mixed-dimensional embedded problems is not sufficient to successfully apply these models to realistic problems. An essential difficulty to overcome is the development of efficient numerical solvers that can handle the large separation of spatial scales between the domains of the equations and the subsequent geometrical complexity of the vascular network.

Actually, the study of the interplay between the mathematical structure of the problem and solvers, as well as preconditioners for its discretization, is still in its infancy. The results presented in [29] for the solution of the $1d$ differential equations embedded in $2d$, and more recently extended to the $3d$-$1d$ case in [28], have paved the way, but much more must be understood. This work proceeds in this direction, with the aim of discussing the main mathematical challenges at the basis of the development of optimal solvers of mixed-dimensional $3d$-$1d$ problems coupled by Lagrange multipliers.

We model the case of one single small vessel by the domain $\Omega \subset \mathbb{R}^3$ that is an open, connected, and convex set that can be subdivided in two parts, $\Omega_\ominus$ and $\Omega_\oplus = \Omega \setminus \overline{\Omega}_\ominus$ representing respectively the vessel and the tissue. Let $\Omega_\ominus$ be a *generalized cylinder* that is the swept volume of a two-dimensional set, $\partial\mathcal{D}$, moved along a curve, Λ, in the three-dimensional domain, Ω, see Figure 1 for an illustration. For dimensional reduction of the vessel domain we finally assume that $|\mathcal{D}| \ll |\Omega|$.

With the purpose of developing robust preconditioners for the *3d-1d* problem arising from microcirculation, let us consider a prototype problem that originates from coupling of two $3d$ second order elliptic equations:

$$\begin{aligned} -\kappa_\oplus \Delta u_\oplus &= f && \text{in } \Omega_\oplus, \\ -\kappa_\ominus \Delta u_\ominus &= f && \text{in } \Omega_\ominus, \\ u_\oplus - u_\ominus &= g && \text{on } \Gamma_\varepsilon, \\ \kappa_\oplus \nabla u_\oplus \cdot \nu_{\Gamma_\varepsilon} - \kappa_\ominus \nabla u_\ominus \cdot \nu_{\Gamma_\varepsilon} &= 0 && \text{on } \Gamma_\varepsilon, \\ u_\oplus,\ u_\ominus &= 0 && \text{on } \partial\Omega. \end{aligned} \tag{1}$$

Here, $u_\oplus$ and $u_\ominus$ are the unknowns, and $\kappa_\oplus > 0$ and $\kappa_\ominus > 0$ are the diffusivities in the two different domains that we shall assume in the following to be constant for simplicity. Furthermore, $\Gamma_\varepsilon = \partial\Omega_\oplus \cap \partial\Omega_\ominus$ where $\varepsilon = \text{diam}\mathcal{D}$ denotes the diameter of the $2d$ transverse cross sections of $\Omega_\ominus$. Finally, f is a forcing term defined in whole Ω and ν_{Γ_ε} denotes the unit normal vector to the surface. The model presented in Equation (1) is a simple template for the interaction of an interior and an exterior domain across the interface Γ_ε. In the context of microcirculation, it appears in many scenarios. For example, it can be used to describe the interaction between blood pressure in small vessels and interstitial fluid pressure. In this case, the variables $[u_\oplus, u_\ominus]$ represent the hydrostatic pressures of a fluid. It can also be adopted to describe the diffusion of chemical species with a small molecular weight (such as oxygen) from the vascular to the extravascular domains. In all cases, we point out that it represents a simplification of more complex phenomena. In the context of oxygen transport, which will be taken as a reference application throughout this work, it is well known that a diffusion-dominated model is not enough to capture the multiphysics nature of blood circulation; indeed, oxygen and hematocrit transport play a significant role in describing the phenomenology. Nevertheless, many numerical approaches for microcirculation tend to solve the equations for oxygen diffusion, convection, and hematocrit separately and in a segregated fashion, see, for example, [18]. In this prospective, the model presented has to be considered as a component of a more comprehensive model. Model (1) also deserves some consideration about the formulation of the coupling conditions. From a physical point of view, $u_\oplus - u_\ominus = g$ on Γ_ε imposes that the oxygen concentration (or partial pressure) is discontinuous throughout the vascular wall. These are the well-known Dirichlet coupling conditions that enforce the value of the solution on some defined portion of the boundary/interface. They are complemented by Neumann-type interface conditions that prescribe the continuity of normal fluxes, that is, $\kappa_\oplus \nabla u_\oplus \cdot \nu_{\Gamma_\varepsilon} - \kappa_\ominus \nabla u_\ominus \cdot \nu_{\Gamma_\varepsilon} = 0$. Dirichlet-Neumann interface conditions are the most fundamental coupling conditions of second-order elliptic PDEs. For this reason, they are our choice here. However, for transport across the wall of small vessels, the model most commonly studied is the Robin coupling [12], which describes the flux at the vessel interface between the vascular and extravascular domains $\Omega_\ominus$, $\Omega_\oplus$, respectively, by the following conditions defined at the interface Γ:

$$-\nabla u_\oplus \cdot \nu_{\Gamma_\varepsilon} = \kappa(u_\oplus - u_\ominus),$$
$$-\nabla u_\ominus \cdot (-\nu_{\Gamma_\varepsilon}) = \kappa(u_\ominus - u_\oplus).$$

Normal oxygen flux at the interface is regulated by the parameter κ, which modulates the permeability of the vessel wall and the relative difference in oxygen concentration between the tissue and the interior of the vessel. However, as it is possible to interpret Robin conditions as a perturbation of the Dirichlet ones, our setting is also relevant for the Robin coupling; see [4].

Imposing Dirichlet boundary conditions via the Lagrange multiplier method can be thought of as imposing boundary conditions on Γ_ε weakly. With reference to Figure 1, and considering the full-dimensional problem (1) for more clarity, the Dirichlet boundary terms coming from the weak formulation of the PDE are replaced by Lagrange multipliers $p_\oplus, p_\ominus \in H^{-1/2}(\Gamma_\varepsilon)$ such that

$$\begin{aligned}\int_{\Gamma_\varepsilon} p_\oplus \, \mathcal{T} v_\oplus \, d\sigma &:= \int_{\Gamma_\varepsilon} (\kappa_\oplus \nabla u_\oplus \cdot \nu_{\Gamma_\varepsilon}) \, \mathcal{T} v_\oplus \, d\sigma \quad \forall v_\oplus \in H^1_0(\Omega_\oplus),\\ \int_{\Gamma_\varepsilon} p_\ominus \, \mathcal{T} v_\ominus \, d\sigma &:= \int_{\Gamma_\varepsilon} (\kappa_\ominus \nabla u_\ominus \cdot \nu_{\Gamma_\varepsilon}) \, \mathcal{T} v_\ominus \, d\sigma \quad \forall v_\ominus \in H^1(\Omega_\ominus).\end{aligned} \tag{2}$$

At this point, introducing the notation $(\cdot,\cdot)_\Sigma$ and $\langle\cdot,\cdot\rangle_\Sigma$ for the L^2 product and duality pairing in domain Σ, the variational formulation of (1) reads:

$$\begin{aligned}&(\kappa_\oplus \nabla u_\oplus, \nabla v_\oplus)_{\Omega_\oplus} + (\kappa_\ominus \nabla u_\ominus, \nabla v_\ominus)_{\Omega_\ominus} +\\ &+ \langle p_\oplus, \mathcal{T} v_\oplus\rangle_{\Gamma_\varepsilon} - \langle p_\ominus, \mathcal{T} v_\ominus\rangle_{\Gamma_\varepsilon} = (f, v_\oplus)_{\Omega_\oplus} + (f, v_\ominus)_{\Omega_\ominus}.\end{aligned}$$

By considering that on Γ_ε we have,

$$\kappa_\oplus \nabla u_\oplus \cdot \nu_{\Gamma_\varepsilon} - \kappa_\ominus \nabla u_\ominus \cdot \nu_{\Gamma_\varepsilon} = 0 \iff \quad p_\oplus = p_\ominus := p,$$

and introducing the weakly imposed Dirichlet boundary constraint

$$\langle \mathcal{T}(u_\oplus - u_\ominus),\, q\rangle_{\Gamma_\varepsilon} = \langle g,\, q\rangle_{\Gamma_\varepsilon} \quad \forall q \in H^{-1/2}(\Gamma_\varepsilon), \tag{3}$$

we obtain the following saddle-point problem

$$\begin{aligned}a([u_\oplus, u_\ominus], [v_\ominus, v_\ominus])_\Omega + b([v_\oplus, v_\ominus], p)_{\Gamma_\varepsilon} &= \langle f, [v_\oplus, v_\ominus]\rangle_\Omega\\ b([u_\oplus, u_\ominus], q)_{\Gamma_\varepsilon} &= \langle g, q_\odot\rangle_{\Gamma_\varepsilon}\end{aligned} \tag{4}$$

for all $[v_\oplus, v_\ominus] \in [H^1_0(\Omega_\oplus), H^1(\Omega_\ominus)],\ q \in H^{-1/2}(\Gamma_\varepsilon)$, where

$$\begin{aligned}a([u_\oplus, u_\ominus], [v_\oplus, v_\ominus]) &= \kappa_\oplus(\nabla u_\oplus, \nabla u_\ominus)_{\Omega_\oplus} + \kappa_\ominus(\nabla u_\ominus, \nabla v_\ominus)_{\Omega_\ominus},\\ b([v_\oplus, v_\ominus], q) &= \langle \mathcal{T}(v_\oplus - v_\ominus), q\rangle_{\Gamma_\varepsilon}.\end{aligned}$$

From the above analysis, we have recovered the saddle-point structure that is inherited by the reduced-dimensionality weak problem (6) from the full-dimensional one. In

this context, the Lagrange multiplier p represents the weighted normal flux $\kappa \nabla u \cdot \nu_{\Gamma_\varepsilon}$ of the variable u. The formulation with the Lagrange multiplier as an auxiliary unknown that enforces the coupling is not the only option when dealing with Dirichlet conditions on the interface. The problem could be addressed, for example, by variants of the penalty method [35] or Nitsche's method [38]. We note that these methods introduce additional (stabilization) parameters into the variational problem.

By applying a suitable model reduction strategy to (1), which exploits the following transverse averages as already described in [31],

$$\overline{w}(s) = |\partial \mathcal{D}(s)|^{-1} \int_{\partial \mathcal{D}(s)} w d\gamma \quad \text{and} \quad \overline{\overline{w}}(s) = |\mathcal{D}(s)|^{-1} \int_{\mathcal{D}(s)} w d\sigma,$$

we obtain the *3d-1d* coupled problem of the form

$$\begin{aligned} -\kappa \Delta u + \varepsilon p_\odot \delta_\Lambda &= f && \text{in } \Omega, \\ -\varepsilon^2 \kappa_\odot d_s^2 u_\odot - \varepsilon p_\odot &= \varepsilon^2 \overline{\overline{f}} && \text{on } \Lambda, \\ \varepsilon(\overline{\mathcal{T}}_\Lambda u - u_\odot) &= g && \text{on } \Lambda, \\ u &= 0 && \text{on } \partial\Omega, \\ u_\odot &= 0 && \text{on } \partial\Lambda. \end{aligned} \tag{5}$$

Here $\kappa = \kappa_\oplus$ in $\Omega_\oplus$ and $\kappa_\odot = \overline{\overline{\kappa}}_\ominus$ in Λ being the centerline of $\Omega_\ominus$. Throughout the paper we will use the subscript $\odot$, e.g. $u_\odot$, for functions on Λ (and, in general, on domains with topological dimension smaller than that of the ambient space), while functions on Ω are denoted, as usual, by italic lowercase letters. Here, the primal unknowns are u and $u_\odot$, while the unknown $p_\odot$ is the Lagrange multiplier used to enforce the coupling of u and $u_\odot$. As a consequence of the dimensionality reduction technique, the Lagrange multiplier $p_\odot$ represents the cross-sectional (perimeter) average of the normal flux of u normal to the vessel interface. Furthermore, δ_Λ is a Dirac delta function. The operator obtained from a combination of the average operator $\overline{(\cdot)}$ with the trace in Γ_ε will be denoted by $\overline{\mathcal{T}}_\Lambda = \overline{(\cdot)} \circ \mathcal{T}_\Gamma$, since it maps functions in Ω to functions in Λ. Note that $\overline{\mathcal{T}}_\Lambda$ thus implicitly depends on ε.

Due to the high-dimensional gap between $3d$ and $1d$, and the presence of singularities in the solution u due to the $1d$ coupling, the well-posedness of the problem (5) is challenging [12, 11]. In the context of Robin coupling conditions at the $3d$-$1d$ interface, the singularity is addressed in a number of works, e.g. by proposing a splitting strategy where the singularity is captured by Green's functions [17], regularizing the problem by distributing the singular source term on the coupling surface or in the bulk [24, 23] or deriving error estimates in tailored norms [25, 11]. For these formulations, efficient solution algorithms have been developed utilizing algebraic multigrid [21, 9] or a fast Fourier transform for preconditioning [47].

Although the Robin coupling typically leads to elliptic problems, enforcing the Dirichlet coupling in (5) by Lagrange multiplier yields a saddle point system. Here, as recently shown in [27], the high $3d$-$1d$ dimensional gap requires the multiplier to reside in fractional order Sobolev spaces on Λ in order to obtain well-posedness.

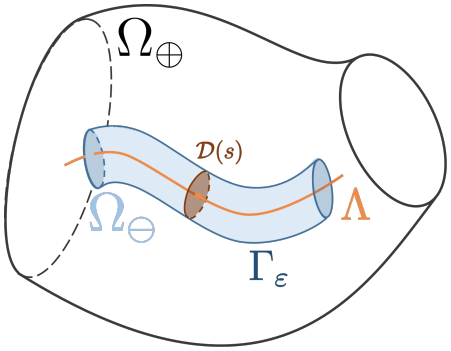

Fig. 1 Geometrical setting considered in this paper, and the associated notation. Domain $\Omega_\ominus$ is assumed to be a slender generalized cylinder characterized by the centerline Λ parameterized by the arclength coordinate s and $2d$ transversal cross section $\mathcal{D}(s)$.

However, scalable solvers for the resulting linear systems are currently lacking. Here, our objective is to address this issue by constructing robust block-diagonal preconditioners for (5) within the framework of operator preconditioning [34]. In particular, to obtain robust estimates we establish the well-posedness of the coupled problem in weighted, fractional Hilbert spaces.

The structure of the chapter is described below. We start with the analysis of the coupled problem in Section 2. Next, we investigate the performance of the resulting preconditioner in Section 3, leading us to the observation that the parameter ε in (5) assumes a distinctive role beyond that of a standard material parameter. This unique role is further examined in Section 4, where we establish a close connection between ε and the well-posedness of the coupled problem. Finally, we provide our conclusions in Section 5.

2 Mathematical formulation of the *3d-1d* coupled problem

Before delving into the precise mathematical formulation of problem (5), we will introduce some fundamental notation. Let D represent a bounded domain in $\mathbb{R}^d$, where $d = 1, 2, 3$. In this context, $L^2(D)$ denotes the space of functions that are square integrable in D, while $H^k(D)$ refers to the space of functions that possess k derivatives in L^2. We denote the closure of $C_0^\infty(D)$ in $H^k(D)$ as $H_0^k(D)$. When the context is clear, we may simplify the notation using H^k instead of $H^k(D)$. For a Hilbert space $X = X(D)$ with its corresponding dual space X', the norm and the associated inner products are denoted as $\|\cdot\|_X$ and $(\cdot,\cdot)_X$, respectively. The duality pairing is represented by $\langle\cdot,\cdot\rangle_X$, and if necessary, we will explicitly indicate the underlying domain using $(\cdot,\cdot)_D$ and $\langle\cdot,\cdot\rangle_D$. With slight abuse of notation, the dual of H^k is H^{-k} for $k \in \mathbb{R}$. Similarly, H_0^{-k} is the dual of H_0^k. We will use scaled and intersected inner products, norms, and Hilbert spaces for our analysis of robustness.

For example $\varepsilon H_0^1(D)$ is defined in terms of the inner product

$$(u,v)_{\varepsilon H_0^1(D)} = \varepsilon^2 (\nabla u, \nabla v)_{L^2(D)}.$$

Notice that with this definition, the norm scales linearly in ε, that is, $\|u\|_{\varepsilon H 1_0} = \varepsilon \|u\|_{H_0^1}$.

The intersection of two Hilbert spaces X and Y is denoted $X \cap Y$ and has an inner product

$$(x,y)_{X\cap Y} = (x,y)_X + (x,y)_Y.$$

We can now precisely formulate the weak formulation of the problem (5) that will be considered in this paper. The problem reads as follows: Find $u \in V, u_\odot \in V_\odot, p_\odot \in Q_\odot$ such that

$$\begin{aligned} a([u,u_\odot],[v,v_\odot]) + b([v,v_\odot],p_\odot) &= \langle f, [v,v_\odot]\rangle_\Omega \qquad \forall [v,v_\odot] \in [V,V_\odot] \\ b([u,u_\odot],q_\odot) &= \langle g, q_\odot\rangle_\Lambda \qquad \forall q_\odot \in Q_\odot. \end{aligned} \tag{6}$$

with

$$\begin{aligned} a([u,u_\odot],[v,v_\odot]) &= \kappa(\nabla u, \nabla u_\odot)_{L^2(\Omega)} + \kappa_\odot \varepsilon^2 (d_s u_\odot, d_s v_\odot)_{L^2(\Lambda)}, \\ b([v,v_\odot],q_\odot) &= \varepsilon \langle \overline{\mathcal{T}}_\Lambda v - v_\odot, q_\odot\rangle_\Lambda \end{aligned}$$

and $V = \kappa^{1/2} H_0^1(\Omega)$, $V_\odot = \kappa_\odot^{1/2} \varepsilon H_0^1(\Lambda)$, and $Q_\odot = \kappa^{-1/2} \varepsilon H^{-\frac{1}{2}}(\Lambda) \cap \kappa_\odot^{-1/2} H^{-1}(\Lambda)$. We remark that a main difference between [27] and the functional setting considered here is that the Lagrange multiplier space $Q_\odot$ is a weighted intersection space $\kappa^{-1/2} \varepsilon H^{-\frac{1}{2}}(\Lambda) \cap \kappa_\odot^{-1/2} H^{-1}(\Lambda)$ rather than $H^{-\frac{1}{2}}(\Lambda)$. This choice is fundamental for the development of robust preconditioners, as will be discussed later on.

2.1 The stability of the continuous problem

We show well-posedness of the variational problem (6) in space $X = V \times V_\odot \times Q_\odot$ considered with its canonical norms by applying the abstract Brezzi theory [6]. To this end, we let

$$\begin{aligned} &A : (V \times V_\odot) \to (V \times V_\odot)', \quad \langle A[u,u_\odot],[v,v_\odot]\rangle_{V\times V_\odot} = a([u,u_\odot],[v,v_\odot]), \\ &B : (V \times V_\odot) \to Q_\odot', \qquad\qquad \langle B[u,u_\odot], q_\odot\rangle_{Q_\odot} = b([u,u_\odot],q_\odot), \end{aligned}$$

such that (6) can be equivalently stated as: Find $x = [u, u_\odot, p_\odot] \in X$ such that

$$\mathcal{A}x = f \text{ in } X', \quad \mathcal{A} = \begin{pmatrix} A & B' \\ B & 0 \end{pmatrix}.$$

The operator $\mathcal{A} : X \to X'$ is then an isomorphism (equivalently, (6) is well posed) provided that it satisfies the four Brezzi conditions, that is, the operators A and B are bounded, A is coercive on $\ker B \subset V \times V_\odot$ and B satisfies the inf-sup condition.

Of the four Brezzi conditions required for the problem (6), the coercivity and boundedness of A were established in [27] in the setting required here ($V \times V_\odot$ are the same and only $Q_\odot$ has changed) and will therefore not be repeated. Therefore, we only need to verify the properties of the B operator.

Theorem 1 *$b(\cdot,\cdot) : [V, V_\odot] \times Q_\odot \to \mathbb{R}$ satisfies the following conditions:*

$$b([u,u_\odot],q_\odot) \le C_B \|[u,u_\odot]\|_{[V,V_\odot]} \|q_\odot\|_{Q_\odot}, \quad u \in V, u_\odot \in V_\odot, q_\odot \in Q_\odot, \tag{7}$$

$$\sup_{[u,u_\odot]\in[V,V_\odot]} \frac{b([u,u_\odot],q_\odot)}{\|[u,u_\odot]\|_{[V,V_\odot]}} \ge \beta \|q_\odot\|_{Q_\odot}, \qquad q_\odot \in Q_\odot \tag{8}$$

with positive constants C_B, β.

Proof We recall that owing to Dirichlet boundary conditions for u, $u_\odot$ we have the equivalence between the seminorms (induced by A) and the full H^1 norms. In [27] the following was established:

$$\varepsilon \|\overline{\mathcal{T}}_\Lambda u\|_{H^{1/2}(\Lambda)} \le C_{\mathcal{T}} \|\mathcal{T}_{\Gamma_\varepsilon} u\|_{H^{1/2}(\Gamma_\varepsilon)} \le C \|u\|_{H^1(\Omega)}, \quad \forall u \in H^1(\Omega),$$

where constants $C_{\mathcal{T}}$ and C are independent from ε. Hence, the boundedness of $b(\cdot,\cdot)$ can be obtained in a direct way as:

$$\begin{aligned}
b([u,u_\odot],q_\odot) &= \varepsilon \langle \overline{\mathcal{T}}_\Lambda u - u_\odot, q_\odot \rangle_\Lambda \\
&\le \varepsilon |\langle \overline{\mathcal{T}}_\Lambda u, q_\odot \rangle_\Lambda| + \varepsilon |\langle u_\odot, q_\odot \rangle_\Lambda| \\
&\le \|\overline{\mathcal{T}}_\Lambda u\|_{H^{1/2}(\Lambda)} \varepsilon \|q_\odot\|_{H^{-1/2}(\Lambda)} + \varepsilon \|u_\odot\|_{H^1(\Lambda)} \|q_\odot\|_{H^{-1}(\Lambda)} \\
&= \kappa^{1/2} \varepsilon \|\overline{\mathcal{T}}_\Lambda u\|_{H^{1/2}(\Lambda)} \kappa^{-1/2} \|q_\odot\|_{H^{-1/2}(\Lambda)} + \varepsilon \kappa_\odot^{1/2} \|u_\odot\|_{H^1(\Lambda)} \kappa_\odot^{-1/2} \|q_\odot\|_{H^{-1}(\Lambda)} \\
&\le \kappa^{1/2} C \|u\|_{H^1(\Omega)} \kappa^{-1/2} \|q_\odot\|_{H^{-1/2}(\Lambda)} + \varepsilon \kappa_\odot^{1/2} \|u_\odot\|_{H^1(\Lambda)} \kappa_\odot^{-1/2} \|q_\odot\|_{H^{-1}(\Lambda)} \\
&\le C_B (\|u\|_V^2 + \|u_\odot\|_{V_\odot}^2)^{1/2} \|q_\odot\|_{Q_\odot}.
\end{aligned}$$

Next, the inf-sup condition reads

$$\sup_{[u,u_\odot]\in[V,V_\odot]} \frac{\varepsilon \langle \overline{\mathcal{T}}_\Lambda u - u_\odot, q_\odot \rangle_\Lambda}{(\|u\|^2_{\sqrt{\kappa} H^1(\Omega)} + \varepsilon^2 \|u_\odot\|^2_{\sqrt{\kappa_\odot} H^1(\Lambda)})^{1/2}} \ge \beta \|q_\odot\|_{Q_\odot}.$$

We first note that $(\alpha X)' = \alpha^{-1} X'$ holds for the dual of weighted Hilbert space. In turn, let R_1 be the Riesz map from $\kappa_\odot^{-1/2} H^{-1}$ to $\kappa_\odot^{1/2} H^1$ and $R_{1/2}$ be the Riesz map from $\kappa^{-1/2} H^{-1/2}$ to $\kappa^{1/2} H^{1/2}$. Then $\hat{u}_\odot = -\frac{1}{\varepsilon} R_1 q_\odot$ implies that $\varepsilon \|\hat{u}_\odot\|_{\sqrt{\kappa_\odot} H^1} = \|q_\odot\|_{\kappa_\odot^{-1/2} H^{-1}}$. From [27], we also see that there exists a harmonic extension operator H such that for $\hat{u} = H\hat{q}_\odot$, $\hat{q}_\odot \in H^{1/2}$. Letting $\hat{q}_\odot = R_{1/2} q_\odot$ we obtain $\hat{q}_\odot = \overline{\mathcal{T}}_\Lambda \hat{u}$ where $\|\hat{q}_\odot\|_{\sqrt{\kappa} H^{1/2}} = \|q_\odot\|_{\kappa^{-1/2} H^{-1/2}}$ and

$$\|\hat{u}\|_{H^1(\Omega)} \leq C_{IT}\varepsilon\|\hat{q}_\odot\|_{H^{\frac{1}{2}}(\Gamma_\varepsilon)} = \varepsilon C_{IT}\|q_\odot\|_{H^{-\frac{1}{2}}(\Gamma_\varepsilon)}.$$

We note that the latter inequality, generally named the *inverse trace inequality*, involves the generic constant C_{IT} that may possibly depend on the domain Γ_ε and precisely on its cross section quantified by the (small) parameter ε. Hence, we obtain

$$\sup_{[u,u_\odot]\in[V,V_\odot]} \frac{\varepsilon\langle\overline{\mathcal{T}}_\Lambda u - u_\odot, q_\odot\rangle_\Lambda}{(\|u\|^2_{\sqrt{\kappa}H^1(\Omega)} + \varepsilon^2\|u_\odot\|^2_{\sqrt{\kappa}_\odot H^1(\Lambda)})^{1/2}} \geq \frac{\varepsilon\langle\overline{\mathcal{T}}_\Lambda\hat{u} - \hat{u}_\odot, q_\odot\rangle_\Lambda}{(\|\hat{u}\|^2_{\sqrt{\kappa}H^1(\Omega)} + \varepsilon^2\|\hat{u}_\odot\|^2_{\sqrt{\kappa}_\odot H^1(\Lambda)})^{1/2}}$$

$$\geq \frac{\varepsilon(\langle R_{1/2}q_\odot, q_\odot\rangle + \langle\frac{1}{\varepsilon}R_1 q_\odot, q_\odot\rangle)}{(C_{IT}\varepsilon^2\|q_\odot\|^2_{\kappa^{-1/2}H^{-1/2}(\Lambda)} + \|q_\odot\|^2_{\kappa_\odot^{-1/2}H^{-1}(\Lambda)})^{1/2}} \geq \beta\|q_\odot\|_{Q_\odot}.$$

□

It should be noted that a proper choice of weighted-intersected Sobolev spaces has led to the removal of any *explicit* dependence of the inf-sup constant β on κ, $\kappa_\odot$ and ε. On the other hand, caution is needed as, through the possible dependence of C_{IT} on ε, the radius may influence β, and in turn the robustness of the estimates in ε.

2.2 Numerical evidence about preconditioning the mixed-dimensional problems

The exploitation of iterative solvers, such as Krylov methods, is crucial to obtain fast solution algorithms for the discretized problems, yet, their performance essentially depends on the existence of a (practical) preconditioner which improves the spectral properties of the linear systems [44]. In constructing preconditioners for the *3d-1d*-problems, a main objective is to establish a parameter robustness preconditioner, i.e. a preconditioner with performance that does not deteriorate with respect to discretization parameters (mesh and element sizes), variations in material parameters ($\kappa > 0$, $\kappa_\odot > 0$) as well as the geometrical parameter ε, crucial for *3d-1d* problems. As an example, in the context of *3d-1d* microcirculation model (5), the radius of the vessel appears explicitly and implicitly in the *3d-1d* problem formulation, as the residue of the link between the three-dimensional topology and the one-dimensional one. Then it must be taken into account.

Here we wish to construct robust preconditioners for the coupled $3d$-$1d$ problem (6) which induces an operator equation: Find $x = [u, u_\odot, p_\odot] \in X$ such that

$$\mathcal{A}x = f \text{ in } X', \quad \mathcal{A} := \begin{pmatrix} -\kappa\Delta & & \varepsilon\overline{\mathcal{T}}_\Lambda{}' \\ & -\kappa_\odot\varepsilon^2\Delta_\Lambda & -\varepsilon I \\ \varepsilon\overline{\mathcal{T}}_\Lambda & -\varepsilon I & 0 \end{pmatrix}, \tag{9}$$

where, for a one-dimensional manifold as Λ, the operator Δ_Λ is equivalent to the second derivative in the direction tangent to Λ, previously denoted as d_s^2.

To establish preconditioners, we follow the framework of operator preconditioning [34]. That is, having shown stability of (6) we define the preconditioner as a Riesz map $\mathcal{B} : X' \to X$ with respect to inner products/norms in which the problem was shown to be well-posed. In turn, the framework relates the conditioning of the (preconditioned) operator $\mathcal{B}\mathcal{A} : X \to X$ to the stability constants of the Brezzi theory. More precisely, independence of the constants with respect to a particular problem parameter translates to robustness of the preconditioner (in the said parameter variations). Note that in case of (6), the critical Brezzi constants are C_B and β related to the boundedness and inf-sup condition of the bilinear form b, cf. Theorem 1. We remark that to obtain a robust discrete preconditioner, stable discretization is required in addition to well-posedness of the continuous problem. In particular, the Brezzi constants of the discretized problem must be independent of the discretization parameter.

Applying operator preconditioning, the analysis of well-posedness in [27] and Theorem 1 yields two different preconditioners for (9). Here, a key difference is the construction of the multiplier space, as [27] considers $H^{-1/2}(\Lambda)$. However, this space does not lead to robust algorithms as we shall demonstrate next. In fact, intersection spaces of Theorem 1 will be needed to obtain robustness in the material parameters. At the same time, at the end of this work it will become clear that the radius ε, as a parameter, plays a special and critical role in the robustness of a preconditioner originating from Theorem 1.

2d-1d preconditioning example

Let us illustrate the challenges of developing a robust preconditioner for mixed-dimensional equations using a $2d$ analogue of (9) where we let $\Lambda = \Lambda_\varepsilon$ be a closed curved contained in the interior of $\Omega \subset \mathbb{R}^2$, cf. Figure 2. Here, the coupling between the problem unknowns defined on Ω and Λ shall be realized by the standard $2d$-$1d$ trace operator leading to the coupled problem: Find $y = [u, u_\odot, p_\odot] \in Y$ such that

$$\mathcal{A}y = f \text{ in } Y', \quad \mathcal{A} = \begin{pmatrix} -\Delta & & \mathcal{T}_\Lambda' \\ & -\kappa_\odot \Delta_\Lambda & -I \\ \mathcal{T}_\Lambda & -I & 0 \end{pmatrix}. \tag{10}$$

Note that (10) is structurally similar to the $3d$-$1d$ coupled problem (9). However, for simplicity, the model $2d$-$1d$ problem contains only a single parameter, $\kappa_\odot > 0$, whose value can be (arbitrarily) large or small. We also recall that Λ is closed, and thus, in order to have an invertible operator on the whole of $H^1(\Lambda)$, we set $-\Delta_\Lambda = -\Delta_\Lambda + I$ in this section. We finally remark that in (9) the Laplacian on Λ is invertible due to boundary conditions imposed on $\partial\Omega_\ominus$ outside the coupling surface.

Following [29] where (10) has been shown to be well-posed with $Y = H_0^1(\Omega) \times H^1(\Lambda) \times H^{-1/2}(\Lambda)$ we shall construct preconditioners as Riesz maps with respect

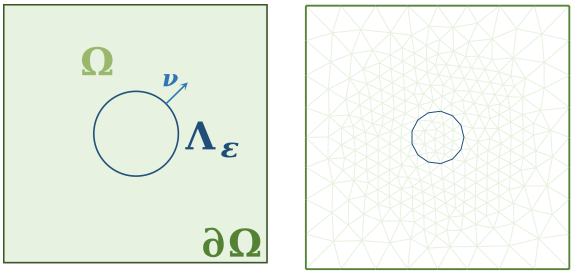

Fig. 2 (Left) Geometrical setting of the *2d-1d* problem (13). Domain Λ_ϵ plays similar role to the centerline in *3d-1d* system (5). (Right) In the experiments triangulation of Ω conforms to Λ.

to two different inner products on Y leading to operators

$$\mathcal{B}_0 = \begin{pmatrix} -\Delta & & \\ & -\kappa_\odot \Delta_\Lambda & \\ & & -\Delta_\Lambda^{-1/2} \end{pmatrix}^{-1}, \quad \mathcal{B}_1 = \begin{pmatrix} -\Delta & & \\ & -\kappa_\odot \Delta_\Lambda & \\ & & -\Delta_\Lambda^{-1/2} - \kappa_\odot^{-1}\Delta_\Lambda^{-1} \end{pmatrix}^{-1}. \tag{11}$$

Here $\mathcal{B}_0$ stems from the analysis in [29] and can be seen to be analogous to the Riesz map preconditioner established in [27] for the coupled $3d$-$1d$ problem (9). In particular, the multiplier block of the preconditioner is a Riesz map of $H^{-1/2}(\Lambda)$ and is independent of the parameter $\kappa_\odot$. On the other hand, with $\mathcal{B}_1$ the multiplier is sought in the intersection space $H^{-1/2}(\Lambda) \cap \kappa_\odot^{-1/2} H^{-1}(\Lambda)$, cf. Theorem 1.

We shall compare the two preconditioners in terms of their spectral condition numbers defined as the ratio between the largest and smallest in magnitude eigenvalues of the problem: Find $y \in Y$, $\lambda \in \mathbb{R}$

$$\mathcal{A} y = \lambda \mathcal{B}_i^{-1} y \quad \text{in } Y'. \tag{12}$$

To assess robustness of the preconditioners we consider the generalized eigenvalue problem (12) for different values of $10^{-8} \leq \kappa_\odot \leq 10^8$ and refinements of the domain $\Omega = (-1, 1)^2$ with $\Gamma_\varepsilon = \{x \in \Omega, |x| = 0.1\}$. We then discretize the problem by continuous linear Lagrange elements ($\mathbb{P}_1$) where the finite element mesh of Ω always conforms to Λ, cf. Figure 2.

Before addressing the preconditioners, let us briefly comment on the approximation property of the chosen discretization. To this end we note that (10) is associated with a system

$$\begin{aligned} -\Delta u &= f && \text{in } \Omega, \\ -\kappa_\odot \Delta_\Lambda u_\odot - [[\nabla u]] \cdot \nu &= f_\odot && \text{on } \Lambda, \\ u - u_\odot &= g && \text{on } \Lambda \end{aligned} \tag{13}$$

which is here supplied with homogeneous Dirichlet boundary conditions for u, $u_\odot$ on $\partial\Omega$ and $\partial\Lambda$ respectively. Here, $[[\cdot]]$ is the jump operator on Λ, $[[v]] = v^+ - v^-$, defined with respect to the normal vector on the curve which points from the positive to the negative side.

Using (13) we measure the convergence of the discrete approximations u_h, $u_{\odot,h}$, $p_{\odot,h}$ in the norms induced by the (symmetric and positive definite) operator $\mathcal{B}_1^{-1}$. Here, the linear systems stemming from discretization[1] by $\mathbb{P}_1$ are solved with a preconditioned MinRes solver using the relative tolerance of 10^{-10}, see also Figure 6.

The approximation errors obtained are plotted in Figure 3, which, for all the values of $\kappa_\odot$, shows linear convergence in the respective H^1-norms for the error in u and $u_\odot$. Quadratic convergence can be seen for the multiplier in the norm of the intersection space $H^{-1/2}(\Lambda) \cap \kappa_\odot^{-1/2} H^{-1}(\Lambda)$. Without including the results, we remark that the intersection norm is essential for obtaining robust approximation. In particular, we observed that measuring convergence in only the $H^{-1/2}$-norm yields quadratic convergence for large values of $\kappa_\odot$ while for small values the rate drops to linear.

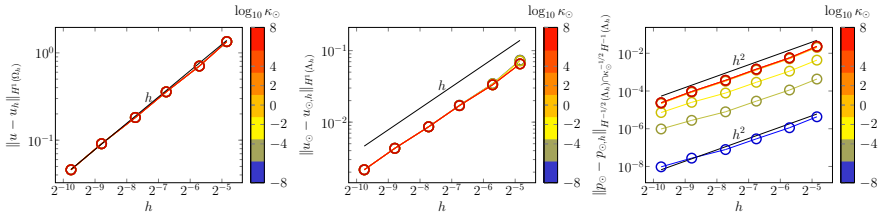

Fig. 3 Approximation errors of $\mathbb{P}_1$ discretization of (10) for different values of $\kappa_\odot$.

Having verified the discretization scheme (and our implementation), we return to preconditioning and stability of the eigenvalue problem (12). We summarize the results in Figure 4 and Figure 5 that show the extrema, that is, the minimum and maximum absolute values of the eigenvalues λ_h of the discretized problem (12). We note that the bounds are plotted together with their sign which carries relevant information related e.g. to the discrete inf-sup or coercivity conditions.

Using $\mathcal{B}_0$, the extremal eigenvalues of (12) are displayed in Figure 4. We observe that for each $\kappa_\odot$ the quantities are bounded in h verifying the stability of the discrete problem with $\mathbb{P}_1$ elements and the norm induced on Y by $\mathcal{B}_0^{-1}$, see [29]. However, there is an apparent growth of the largest eigenvalue in magnitude as $\kappa_\odot$ becomes small. As such, $\mathcal{B}_0$ does not produce a robust parameter solver. On the other hand, the preconditioner $\mathcal{B}_1$ yields spectral bounds that are stable in $\kappa_\odot$ and mesh refinement. We note that for small $\kappa_\odot$ the observed upper and lower bounds are close to their theoretical values [36, 43] of $(1+\sqrt{5})/2$ and $(1-\sqrt{5})/2$ respectively. This is due to the multiplier norm being then dominated by the matrix of the H^{-1}-inner product such that the discrete preconditioner (which computes $-\Delta_\Lambda^{-1}$ by LU decomposition) is close to being the exact Schur complement preconditioner.

To illustrate how conditioning translates into performance of iterative solvers, Figure 6 reports the iteration counts of the MinRes solver using the two preconditioners (11). Here, we reuse the setup of the previous eigenvalue experiments while

[1] In all the presented numerical examples FEniCS[33]-based module FEniCS$_{\text{ii}}$[26] was used to discretize the coupled problems.

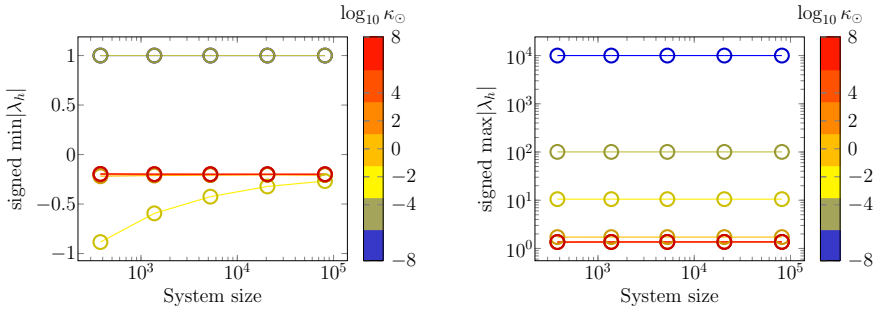

Fig. 4 Performance of preconditioner $\mathcal{B}_0$ from (11) for problem (10) with varying $\kappa_\odot$. Here $\Omega = (-1,1)^2$, Γ_ε is a circle of radius $\varepsilon = 0.1$. All finite element spaces are discretized by $\mathbb{P}_1$ elements. The preconditioner does not produce $\kappa_\odot$-bounded condition numbers.

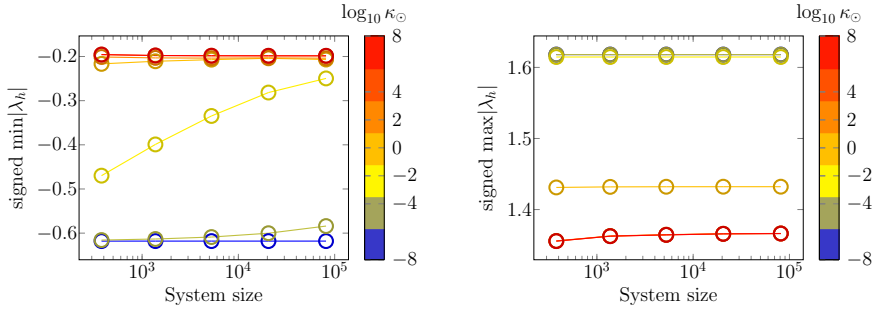

Fig. 5 Performance of preconditioner $\mathcal{B}_1$ from (11) for $2d$-$1d$ coupled problem (10) with varying $\kappa_\odot$. Setup as in Figure 4. The preconditioner is robust in $\kappa_\odot$ and in mesh size.

the right-hand side f in (10) is based on the manufactured solution setup described above. For each value of $\kappa_\odot$ and the mesh size, the solver starts from 0 initial guess and ends once the preconditioned residual norm is reduced by factor 10^{10}. Both preconditioners are computed exactly using LU for the two leading blocks, while the multiplier block, in particular the fractional term $-\Delta_\Lambda^{-1/2}$ is realized via spectral decomposition[2], see [29] for a precise definition.

In Figure 6 it can be seen that for large values of $\kappa_\odot$ both preconditioners yield iterations which are stable in mesh refinement. However, for small values, that is, when the term $\kappa_\odot^{-1}\Delta_\Lambda^{-1}$ becomes large, $\mathcal{B}_0$ shows a dependence on the parameter. We conclude that the intersection space exploited in the definition of $\mathcal{B}_1$ is crucial for parameter robustness.

[2] Spectral decomposition is not suitable for practical applications because of its cubic scaling. However, Riesz maps at intersections of fractional-order Sobolev spaces can be approximated with optimal complexity by rational approximations [7].

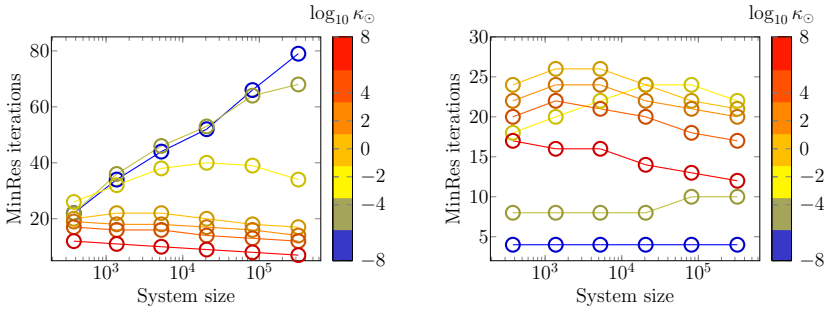

Fig. 6 Convergence of (11)-preconditioned MinRes solver for the problem (10) with varying $\kappa_\odot$. Only the preconditioner $\mathcal{B}_1$ (right) reflecting $p_\odot \in H^{-1/2} \cap \kappa_\odot^{-1/2} H^{-1}$ is parameter robust. Setup as in Figure 4.

3 Definition of a preconditioner for the *3d-1d* problem: performances and drawbacks

At this point let us return to the original coupled $3d$-$1d$ problem (9) that we shall now consider with a preconditioner

$$\mathcal{B} = \begin{pmatrix} -\kappa\Delta & & \\ & -\kappa_\odot \varepsilon^2 \Delta_\Lambda & \\ & & -\frac{\varepsilon^2}{\kappa}\Delta_\Lambda^{-1/2} - \kappa_\odot^{-1}\Delta_\Lambda^{-1} \end{pmatrix}^{-1}, \tag{14}$$

i.e. the Riesz operator associated to the inner product of the space in which well-posedness of (9) was shown in Theorem 1. We note that for the approximate inversion of the diagonal blocks of (14), optimal algorithms are widely recognized in numerous instances, such as multigrid, domain decomposition, and Fast Fourier Transform (FFT) methods, particularly for standard Riesz maps in H^1, $H(\mathrm{div})$, $H(\mathrm{curl})$, etc. Given the widespread recognition of these methods in the field, providing references might be superfluous as these concepts are generally well established and well known. Moreover, recent developments have extended optimal algorithms to encompass fractional operators, broadening the applicability and efficiency of these numerical strategies [2, 16, 5, 8].

In order to test (14) we consider cylindrical domains $\Omega_\oplus$, $\Omega_\ominus$ each with height 1 and radii of 0.5 and ε respectively. Following [27] we discretize $\Omega = \Omega_\oplus \cup \Omega_\ominus$ so that the mesh conforms both to the interface Γ_ε and the centerline Λ, see Figure 7. We remark that the conformity assumption was used in [27] to show stability of the discrete problem with $\mathbb{P}_1$ elements (used below). At the same time, the assumption leads to greatly refined meshes in the vicinity of Γ_ε. It also increases the cost of mesh generation and, due to the size of the resulting system, restricts[3] the type of

[3] As an example, for radius $\varepsilon = 1 \cdot 10^{-2}$ the finest mesh considered contained roughly 11 million tetrahedra. Using $\mathbb{P}_1$ elements, the number of $3d$ unknowns is then ~2 million, while the multiplier space has ~2 thousand degrees of freedom.

experiments we can perform (on our serial computational setup). In the following we shall thus limit the computational study only to robustness of iterative methods. We note that stable discretization of (14) is also possible if the mesh of Ω is independent of Λ and Γ, cf. [27]. However, we argue that the conforming setup is simpler and more transparent.

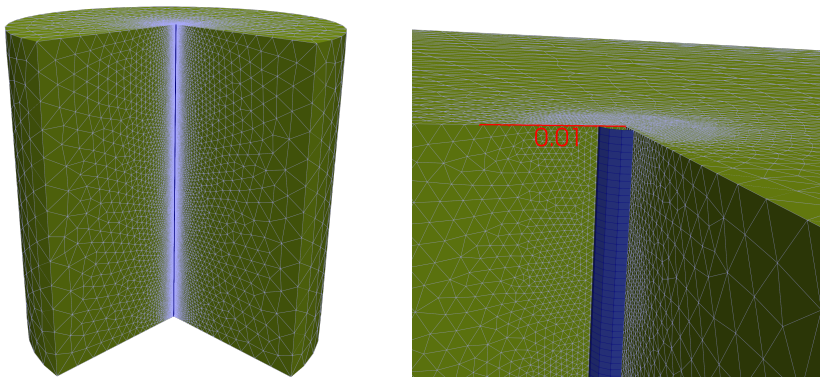

Fig. 7 Computational mesh considered in experiments for the coupled $3d$-$1d$ problem (14). Here $\varepsilon = 2 \cdot 10^{-3}$. The mesh of Ω conforms to the centerline Λ and to the coupling surface Γ_ε leading to high refinement near Λ (the edges of the mesh elements are colored light blue). (Right) The virtual surface used to calculate $\overline{\mathcal{T}}_\Lambda$ is rendered in dark blue color.

In Figure 8 we report on the convergence of the MinRes solver using the preconditioner (14) for the $2 \cdot 10^{-3} \leq \varepsilon \leq 10^{-1}$ and two-parameter regimes. Here, the action of the leading block $-\kappa\Delta^{-1}$ of (14) is approximated in terms of (i) a single V-cycle of algebraic multigrid (AMG) and (ii) 10 steps of the preconditioned conjugate gradient (PCG) method using AMG as preconditioner. The remaining two blocks of (14) are computed by LU factorization. We remark that choice (i) is more practical, while with (ii) the preconditioner is almost exact as the absolute residual norm after the 10 PCG steps is typically $< 10^{-15}$ in our case. With the case (ii) we thus aim to ensure that the effects of parameter variations on MinRes convergence are (mostly) due to the construction of the multiplier preconditioner. In both cases, the convergence criterion for the MinRes solver requires reducing the preconditioned residual norm by a factor 10^{10}. Finally, the coupling operator $\overline{\mathcal{T}}_\Lambda$ is approximated using a Legendre quadrature of degree 20.

Taking into account the results in Figure 8 we observe that the performance of the preconditioner differs dramatically between the two regimes. When $\kappa = 10^8$, $\kappa_\odot = 10^{-8}$, such that the H^{-1}-term can dominate the multiplier block in $\mathcal{B}$, the iteration counts are practically independent of ε. Note that here only the construction (i) for the leading block is considered, as it already yields low enough iterations. On the other hand, with $\kappa = 10^{-8}$, $\kappa_\odot = 10^8$ the solver performance deteriorates for small radii. This is true for the construction (i) which, for the different radii $\varepsilon \in \left\{1 \cdot 10^{-1}, 5 \cdot 10^{-2}, 1 \cdot 10^{-2}, 5 \cdot 10^{-3}, 2 \cdot 10^{-3}\right\}$ and the finest refinement levels,

yields the iteration counts of 37, 44, 58, 71, 100 as well as for (ii) where convergence is reached respectively after 28, 31, 40, 46, 68 iterations.

The unbounded iterations, in particular with preconditioner (ii), bring into question the stability of the coupled $3d$-$1d$ problem (9) with preconditioner (14) and in particular the intersection space $Q_\odot$ for the multiplier. The lack of robustness is surprising, as it suggests that radius ε in (9) does not behave as a standard material parameter in the sense that the corresponding weighting in the (appropriate) intersection space does not yield robustness with respect to its variations. However, this result may be qualitatively justified on the basis of stability analysis, where we noticed the influence of the constant C_{IT} on the inf-sup condition. In the next section, we will show that C_{IT} may depend on ε, which may explain the findings in Figure 8.

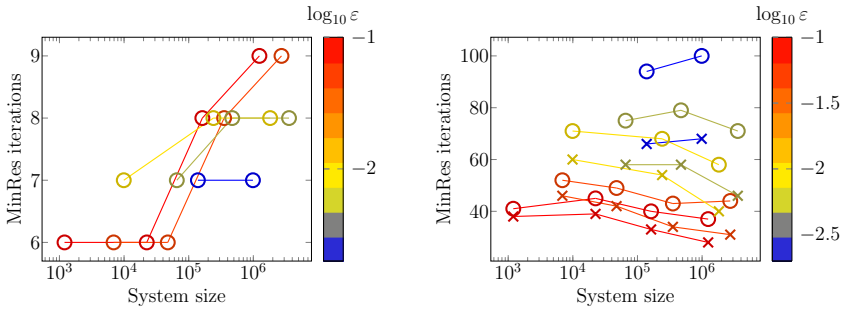

Fig. 8 Performance of preconditioner (14) for the coupled $3d$-$1d$ problem (9) and varying radius. (Left) We set $\kappa = 10^8$, $\kappa_\odot = 10^{-8}$. (Right) We set $\kappa = 10^{-8}$, $\kappa_\odot = 10^8$. The leading block of the preconditioner uses single AMG V-cycle ($\circ$ markers) or 10 PCG iterations with AMG preconditioner ($\times$ markers). The remaining blocks are realized by LU.

Varying radius in *2d-1d* preconditioning example

In order to gain more insight into the observation that in the $3d$-$1d$ setting of (9) the multiplier preconditioner reflecting the intersection space $\kappa^{-1/2}\varepsilon H^{-1/2} \cap \kappa_\odot^{-1/2} H^{-1}$ did not lead to robustness, let us return to the $2d$-$1d$ operator (10). Next, we investigate the properties of the preconditioner $\mathcal{B}_1$ when ε varies. We recall that $\mathcal{B}_1$ was found to be robust with respect to the material parameters.

Using the previous experimental setup, Figure 9 shows the performance of the preconditioner when $\kappa_\odot = 10^{10}$ and $\varepsilon \leq 10^{-1}$. Here, by choosing a large $\kappa_\odot$ we wish to put emphasis on the fractional part of the multiplier preconditioner, which, analogously to Theorem 1, brings the inverse trace constant into the Brezzi estimates. In Figure 9 we observe that while the largest eigenvalues are bounded in ε, the smallest in magnitude eigenvalue approaches 0 as Λ_ε shrinks. We note that for all ε the two eigenvalue bounds are stable in mesh size h. In the figure, we further report convergence history of the MinRes solver (run with the same settings as in the previous experiments). We observe that for small radii the iteration counts grow

rapidly with initial mesh refinement before decreasing back on finest meshes, cf. bounded iterations with mesh refinement in Figure 6. However, the limit $\varepsilon \to 0$ does not seem to affect the iterative solver as clearly as blow-up of the condition number, cf. $\min|\lambda_h|$ in Figure 9. We attribute this behavior to the specific choice of the right-hand side and 0 initial guess in our numerical setup. However, the sensitivity to the radius furthers our claim of the special role of ε in understanding the robustness of the preconditioner.

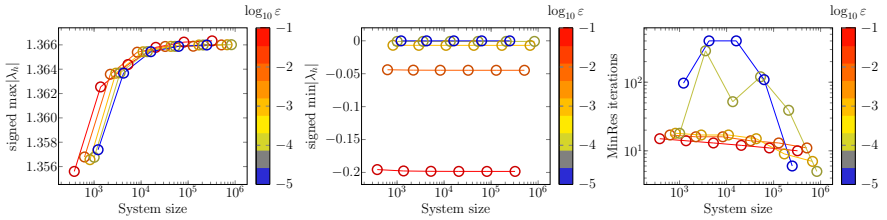

Fig. 9 Performance of preconditioner $\mathcal{B}_1$ in (11) for problem (10) with $\kappa_\odot = 10^{10}$, $\Omega = (-1, 1)^2$, Γ_ε is a circle of radius $10^{-5} \leq \varepsilon \leq 10^{-1}$. All finite element spaces are discretized by $\mathbb{P}_1$ elements. (Left, center) The conditioning deteriorates with ε as the largest in magnitude eigenvalue (12) is bounded in the parameter while the smallest in magnitude eigenvalue decreases with ε. (Right) For small radii the iterations are not stable (the maximum number of allowed iterations is set to 400).

4 The role of the inner radius on mixed-dimensional problems

As discussed in the previous sections, it has been observed that the robustness of the preconditioner (14) decreases as the inner radius of the inclusion approaches zero. This behavior is not limited to the $3d$-$1d$ preconditioner formulation but is also evident in the $2d$-$1d$ examples. Consequently, it suggests that the detrimental effect of ε is not the result of the dimensional reduction technique itself, but rather inherent in the mathematical structure of the problem.

Specifically, the dependence on ε is manifested in the constant of the inf-sup stability property. The analysis in Theorem 1 reveals that the boundedness constant C_B of the bilinear form b remains independent of the inner diameter. However, the inf-sup constant β is not guaranteed to be independent of ε as the presence of the inverse trace constant C_{IT} introduces questions regarding its independence from the inner radius. The inverse trace theorem, a well-established result in functional analysis, provides insight into this matter (see, for example, [46], [37], [32]). However, deriving an accurate bound for C_{IT} is a challenging task, particularly when considering a parameterized domain.

In this section, our objective is to investigate the relationship between the inf-sup constant β and the parameter ε, which is closely associated with the inverse trace constant C_{IT}. To accomplish this, we analyze a simplified yet significant scenario

that allows us to elucidate the connection between the inf-sup constant and the inner radius.

4.1 The 2*d*-1*d* formulation for the perforated domain problem

Consider a generalized cylindrical vessel immersed in a three-dimensional domain Ω. The surface of the vessel is indicated by Γ_ε, where ε indicates the radius of the cylinder. We are interested in studying how the mathematical structure of the problem behaves when $\varepsilon \to 0$. A straightforward approach can be to select a slice of Ω, here denoted by the superscript "$*$", such that we obtain a domain Ω^*, where the curve Γ^*_ε is the restriction of Γ_ε on the slice, see Figure 10. Clearly, $\mathrm{diam}\Gamma^*_\varepsilon$ depends on ε. In turn, studying the effects of shrinking $\mathrm{diam}\Gamma^*_\varepsilon$ in Ω^* (a $2d$-$1d$ system) is representative of the effects of the decreasing vessel / inner radius. The underlying assumption is the complete decoupling of the radius influence from the axial direction, which seems reasonable when considering a cylindrical setting. Indeed, inspecting the expression of the Laplacian in cylindrical coordinates

$$\Delta = \frac{1}{\rho}\frac{\partial}{\partial\rho}\left(\rho\frac{\partial}{\partial\rho}\right) + \frac{1}{\rho^2}\frac{\partial^2}{\partial\phi^2} + \frac{\partial^2}{\partial z^2}$$

corroborates the assumption: ρ (and in turn ε) does not appear in the axial derivative part. From now until the end of this section, the superscript "$*$" will be omitted, so

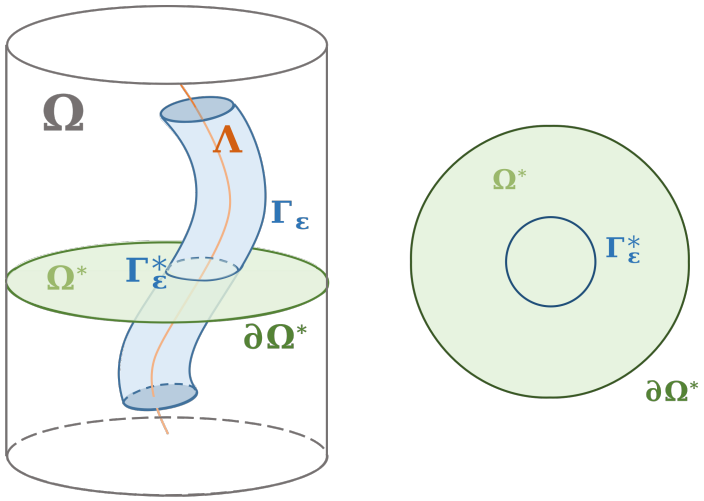

Fig. 10 (Left) Pictorial representation of a vessel with radius ε, centerline Λ and boundary Γ_ε immersed in a three-dimensional domain Ω. By cutting a slice of Ω, we obtain the two-dimensional domain Ω^* with boundary $\partial\Omega^*$ and circular inclusion in one-dimensional Γ^*_ε. (Right) Pictorial representation of the slice domain Ω^*.

that Ω and $\partial\Omega$ will refer respectively to the $2d$ sliced domain and its outer boundary. Moreover, Γ_ε will denote the closed one-dimensional curve embedded in Ω^*.

Let us consider the following ε-dependent Poisson problem defined in Ω:

$$\begin{aligned} -\Delta u &= 0 \qquad \text{on } \Omega, \\ u|_{\Gamma_\varepsilon} &= g \qquad \text{on } \Gamma_\varepsilon, \\ u &= 0 \qquad \text{on } \partial\Omega, \end{aligned} \tag{15}$$

where $\Gamma_\varepsilon \cap \partial\Omega = \emptyset$ and u is a two-dimensional scalar field defined on Ω. Now consider a mixed weak formulation of (15), where the boundary condition on Γ_ε is weakly enforced by a Lagrange multiplier to allow the mathematical structure of (15) to mirror the $3d$-$1d$ problem. The variational problem reads:

$$\begin{aligned} (\nabla u, \nabla v)_\Omega + (p_\odot, \mathcal{T} v)_{\Gamma_\varepsilon} &= 0 \qquad && \forall u, v \in H^1_0(\Omega) \\ (\mathcal{T} u, q_\odot)_{\Gamma_\varepsilon} &= (g, q_\odot)_{\Gamma_\varepsilon} \qquad && \forall p_\odot, q_\odot \in H^{-1/2}(\Gamma_\varepsilon) \end{aligned}. \tag{16}$$

Note that the solution operator $\mathcal{A}$ of (16) has the following block structure

$$\mathcal{A} = \begin{pmatrix} A & B' \\ B & 0 \end{pmatrix}, \quad \langle Au, v\rangle_\Omega = \int_\Omega \nabla u \cdot \nabla v, \quad \langle Bu, q_\odot\rangle_{\Gamma_\varepsilon} = \int_{\Gamma_\varepsilon} p_\odot v.$$

The question we will address next is that of the well-posedness of the variational formulation (16) when $\varepsilon \to 0$. In the framework of saddle-point problems, the boundedness of the bilinear forms a, b in the case of (16) can be easily established with the respective constants equal to 1. Regarding the existence of the Brezzi inf-sup constant β, a straightforward proof will make use of the following theorem [46]:

Theorem 2 ***(Inverse Trace Theorem)*** *Given the necessary smoothness assumption for Ω, the trace operator $\mathcal{T} : H^1(\Omega) \to H^{1/2}(\Gamma_\varepsilon)$ has a continuous right inverse operator*

$$\mathcal{E} : H^{1/2}(\Gamma_\varepsilon) \to H^1(\Omega)$$

satisfying $\mathcal{T}\mathcal{E} w_\odot = w_\odot$ for all $w_\odot \in H^{1/2}(\Gamma_\varepsilon)$ as well as

$$\|\mathcal{E} w_\odot\|_{H^1(\Omega)} \le C_{IT} \|w_\odot\|_{H^{1/2}(\Gamma_\varepsilon)} \quad \forall w_\odot \in H^{1/2}(\Gamma_\varepsilon).$$

Then, by taking $v = \mathcal{E} v_{q_\odot}$, where, by $v_{q_\odot}$, we intend an element of $H^{1/2}(\Gamma_\varepsilon)$ such that the following Riesz mapping properties hold

$$\langle v_{q_\odot}, w_\odot\rangle_{H^{1/2}(\Gamma_\varepsilon)} = (q_\odot, w_\odot)_{\Gamma_\varepsilon} \text{ and } \|v_{q_\odot}\|_{H^{1/2}(\Gamma_\varepsilon)} = \|q_\odot\|_{H^{-1/2}(\Gamma_\varepsilon)},$$

we obtain that

$$\begin{aligned} \sup_{v \in H^1_0(\Omega), v \neq 0} \frac{(\mathcal{T} v, q_\odot)_{\Gamma_\varepsilon}}{\|v\|_{H^1_0(\Omega)}} &\ge \frac{(v_{q_\odot}, q_\odot)_{\Gamma_\varepsilon}}{\|\mathcal{E} v_{q_\odot}\|_{H^1_0(\Omega)}} \\ &= \frac{\langle v_{q_\odot}, v_{q_\odot}\rangle_{H^{1/2}(\Gamma_\varepsilon)}}{\|\mathcal{E} v_{q_\odot}\|_{H^1_0(\Omega)}} \ge \frac{1}{C_{IT}} \|v_{q_\odot}\|_{H^{1/2}(\Gamma_\varepsilon)}. \end{aligned}$$

What is apparent from the above calculation is, again, the structural relationship between the existence of the inf-sup constant β, and the inverse trace inequality constant C_{IT} i.e $\beta = 1/C_{IT}$. This suggests (and is what we want to uncover) a tight relationship between β and the inner radius using the *trace inequality constant* C_T. Indeed, from Lemma 2.2 in [24], the influence of ε is made clear:

Lemma 1 (Lemma 2.2 in [24]) *Let $B_\varepsilon \subset \mathbb{R}^2$ be a circle with a sufficiently small radius ε and $v \in H_0^1(\Omega)$. Then we have:*

$$\|\mathcal{T}v\|_{L^2(\partial B_\varepsilon)} \leq C_T \|v\|_{H_0^1(\Omega)} = C\sqrt{\varepsilon|\log\varepsilon|}\,\|v\|_{H_0^1(\Omega)} \tag{17}$$

with C positive and independent of ε.

Considering that the extension operator, $\mathcal{E}$, is the right inverse of the trace, $\mathcal{T}$, the following claim is proposed: *the radius of the vessel ε directly affects the inf-sup constant β through the constant of the inequality of the trace C_T*. This claim sounds reasonable if one considers that β directly characterizes the lower bound of the bilinear form b, which strongly depends on the trace operator; moreover, it is corroborated by the fact that $\beta = 1/C_{IT}$ so that, assuming a relation between the trace inequality and the inverse trace one, we find that ε directly affects β. However, to prove the claim, it would be required to track in detail the exact expression of C_{IT}, thus obtaining a direct link between β and ε. Establishing such an analytical expression for C_{IT} can be a very intricate task, especially when the domain size needs to be considered as a parameter. Nevertheless, we can rely on numerical analysis and employ the computability of the constants in a discretized setting, as follows.

Brezzi inf-sup constant evaluation. Let $V = H_0^1(\Omega)$, $Q = H^{-1/2}(\Gamma_\varepsilon)$ and $\|\cdot\|_V$ be the H_0^1-norm (induced by the operator A) while $\|\cdot\|_Q$ shall be the $H_\Gamma^{-1/2}$-norm induced by the fractional operator $N := (-\Delta + I)^{-1/2}$ (where both terms are understood to be defined in Γ_ε). Consider now a family (V_h, Q_h) of discretization of (V, Q) characterized by the following discrete Brezzi inf-sup constant.

$$\sup_{v\in V_h, v\neq 0} \frac{b(v, q_\odot)}{\|v\|_{V_h}} \geq \beta_h \|q_\odot\|_{Q_h} \quad \forall q_\odot \in Q_h. \tag{18}$$

If (V_h, Q_h) is a *stable* discretization i.e. both the discrete Brezzi inf-sup and coercivity constants are bounded from below by a constant which is independent from h [1], [42]:

$$\{\beta_h\}_{h\to 0} \geq \beta > 0, \tag{19}$$

then an approximation of β can be obtained by considering the truncated limit $\{\beta_h\}_{h\to\delta}$, for δ sufficiently small. For the purpose of computing β_h, we recall the following lemma of Qin [41]:

Lemma 2 (Qin [41]) *Given a stable discretization (V_h, Q_h) for the saddle point problem* (16)*, consider the following generalized eigenvalue problem: Find $\lambda \in \mathbb{R}$, $0 \neq (u, p_\odot) \in V_h \times Q_h$ such that*

$$\langle u_h, v\rangle_V + b\left(v, p_\odot\right) + b\left(u_h, q_\odot\right) = -\lambda \left\langle p_\odot, q_\odot\right\rangle_Q \quad \forall (v, q_\odot) \in V_h \times Q_h. \tag{20}$$

Then, $\lambda \geq 0$ *and* $\beta \approx \beta_h = \sqrt{\lambda^{\min}}$.

In the framework of the problem (16), the eigenvalue problem can be resolved in the following form involving the Schur complement of $\mathcal{A}$: Find $p_\odot \in Q_h$, $\lambda_B > 0$ such that[4]

$$BA^{-1}B' p_\odot = \lambda_B^2 N p_\odot \quad \text{in } Q_h'. \tag{21}$$

Here, the subscript B, which stands for "Brezzi", has been introduced for clarity of notation, as will become clear soon. In particular, for stability of the discrete problem (16), $\lambda_B^{\min} = \min \lambda_B$, $\lambda_B^{\max} = \max \lambda_B$ shall be independent of the mesh size h. We remark that in this framework $\lambda_B^{\min} \approx \beta$.

Trace constant evaluation. Let us consider the eigenvalue problem defined on the domain in Figure 10, which reads as follows:

$$\begin{aligned} -\Delta u &= 0 && \text{in } \Omega \subset \mathbb{R}^2, \\ \nabla u \cdot \nu &= \lambda_S^{-2} u && \text{on } \Gamma_\varepsilon, \\ u &= 0 && \text{on } \partial\Omega, \end{aligned} \tag{22}$$

where ν is the unit normal to Γ_ε. We remark that (22) is a variant of the Steklov eigenvalue problem. For rigorous mathematical treatment of (22) we refer to e.g. [20] and references therein.

The weak formulation of (22), leads to the generalized eigenvalue problem: Find $u \in H_0^1(\Omega)$, $\lambda_S > 0$ satisfying

$$\int_{\Gamma_\varepsilon} uv = \lambda_S^2 \int_\Omega \nabla u \cdot \nabla v \quad \forall v \in H_0^1 \tag{23}$$

so that, $\lambda_S^{\max}$ allows for estimates of the $L^2(\Gamma_\varepsilon)$-norm of u in terms of the $H_0^1(\Omega)$-norm. Indeed, we have $\|u\|_{L^2(\Gamma_\varepsilon)} \leq \lambda_S^{\max} \|u\|_{H_0^1}(\Omega)$ for all $u \in H_0^1(\Omega)$.

Once the eigenvalue problems (20), (22) are properly discretized (from now on, the subscript h will denote the discretized analogues of a given quantity; subscript ε_i will denote a quantity evaluated on a domain with inner/inclusion radius equal to ε_i), the numerical tools for the evaluation of the inf-sup constant β and the trace inequality constant C_T are readily established. Therefore, we can proceed with the investigation of the influence of ε in the mathematical framework considered.

The research path is summarized in Figure 11. Due to the analytical difficulty in the evaluation of the role of the inner radius in the inverse trace constant C_{IT}, and

[4] Though it is λ_B^2 that is the eigenvalue of (21) we shall in the following, with a slight abuse of notation, refer to $\max \lambda_B = \lambda_B^{\max}$, $\min \lambda_B = \lambda_B^{\min}$ as the eigenvalue bounds, extremal eigenvalues or simply eigenvalues. This choice is intended to simplify the notation and avoid proliferation of $\sqrt{}$ in the text. A similar convention will be applied also to the Steklov eigenvalue problems (22) and (26).

its relationship with the trace constant, we shift our inquiry to a discretized setting and the discrete eigenvalue problems. What will be done is a concomitant evaluation of $\{\beta_{h,\varepsilon_i}\}_{\varepsilon_i \in I}$ and $\{C_{T_{h,\varepsilon_i}}\}_{\varepsilon_i \in I}$, where $I = \{\varepsilon_0, \varepsilon_1, \ldots, \varepsilon_n\}$ and $\varepsilon_0 > \varepsilon_1 > \ldots > \varepsilon_n$ with $\varepsilon_n \ll 1$. Then, if there is some noticeable correlation between $\lambda_B^{\min}$ and $\lambda_S^{\max}$ exists, then it also holds for $\{\beta_{h,\varepsilon_i}\}$ and $\{C_{T_{h,\varepsilon_i}}\}$ (by means of (20), (21)) so that we can find numerical evidence to support our claim.

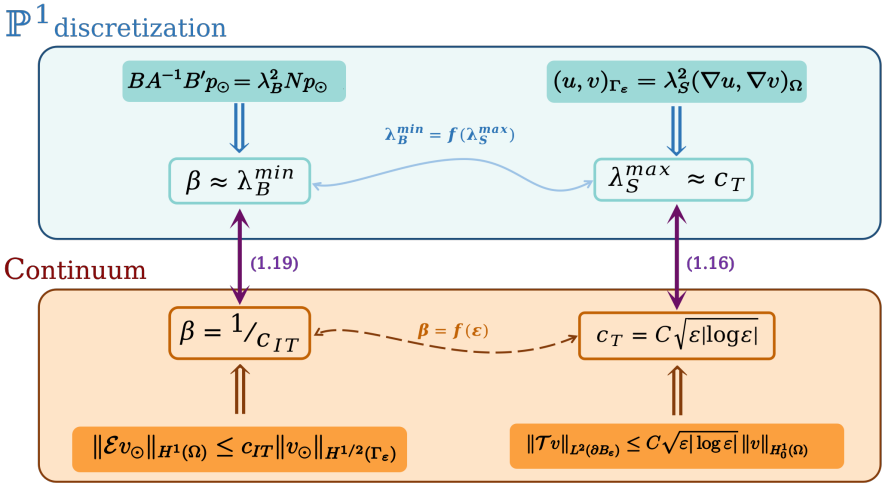

Fig. 11 Pictorial representation of the path followed in the analysis of the role of ε on β. Thanks to the evaluation of the eigenvalues of problems (21) and (22), a relation can be established between $\lambda_B^{\min}$ and $\lambda_S^{\max}$. Then, by virtue of equations (17) (23) (represented by the purple arrows) bridging the discrete setting to the continuous one, we can close the loop and determine a relation between the Brezzi inf-sup constant β and the inner radius ε.

4.2 Numerical results about the 2*d*-1*d* formulation

Here we summarize the numerical experiments concerning the evaluation of $\{\beta_{h,\varepsilon_i}\}$ and $\{C_{T_{h,\varepsilon_i}}\}$ with varying $\varepsilon_i \in I = \{10^{-1}, \ldots, 10^{-5}\}$. For simplicity we shall first limit the investigations to $\Omega = \{x \in \mathbb{R}^2, |x| < 1\}$, a circular inclusion $\Gamma_\varepsilon = \{x \in \Omega, |x| = \varepsilon\}$ and $\mathbb{P}_1$ discretization.

In Figure 12 we demonstrate that our choice of norms and finite element spaces yields a stable problem. More precisely, we observe that both the upper and lower bounds on the Schur complement spectra are stable in mesh refinement for each fixed ε. Moreover, $\lambda_B^{\max}$ appears to be bounded in the radius of Γ_ε, cf. Theorem 1. On the other hand, $\lambda_B^{\min}$ seems to decrease together with ε.

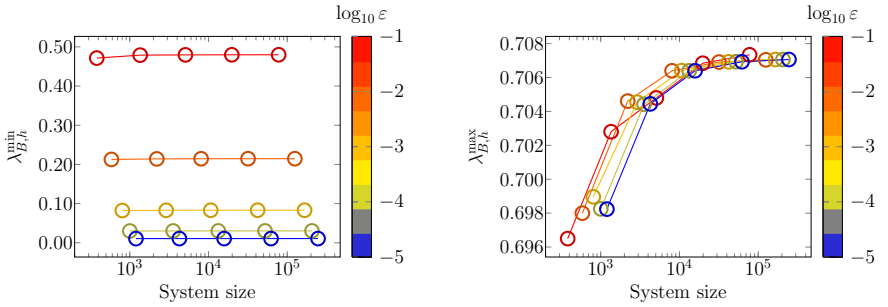

Fig. 12 (Left) Mesh convergence of the extremal eigenvalues of Schur complement (21) for $\Omega = \{x \in \mathbb{R}^2,\ |x| < 1\}, \Gamma_\varepsilon = \{x \in \Omega,\ |x| = \varepsilon\}$. Both spaces V and Q are discretized by $\mathbb{P}_1$ elements. For each ε a sequence of problems is considered on uniformly refined meshes starting from size $h_0 \geq h_l \geq h_{\min}$ leading to eigenvalues λ_{B,h_l}.

We now propose that $\lambda_B^{\min}$ is closely related to the Steklov eigenvalue problem (23). To investigate the relation between $\lambda_S^{\max}$ and $\lambda_B^{\min}$, Figure 13 plots the relative error between the two quantities[5] for varying values of ε. With the relative error $\sim 10^{-4}$ it appears that $\lambda_S^{\max} = \lambda_B^{\min}$. In Figure 13 we finally plot the dependence of $\lambda_S^{\max}$, $\lambda_B^{\min}$ on the radius of Γ_ε. The observed dependence agrees well with the theoretical bound [24].

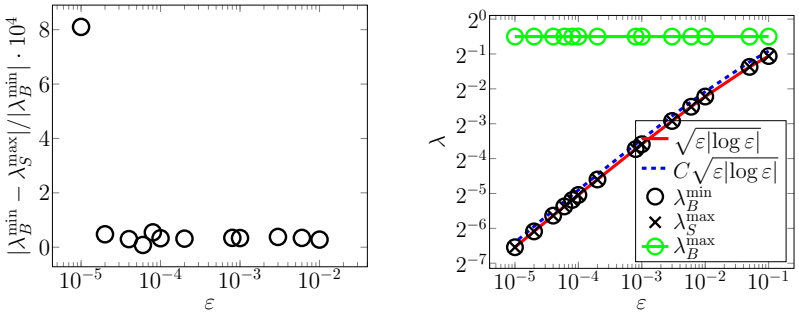

Fig. 13 (Left) Error between the smallest eigenvalue $\lambda_B^{\min}$ of the Schur complement problem (21) and the largest eigenvalue $\lambda_S^{\max}$ of the Steklov problem (23). In both cases, values from the finest level of refinement are considered, i.e. $\lambda_X := \lambda_{X,h_{\min}}$. (Right) Dependence of the Schur complement eigenvalues on the radius of coupling curve $\Gamma_\varepsilon = \{x \in \Omega, |x| = \varepsilon\}$. Value $C \approx 0.999$ is obtained by fitting values $\lambda_B^{\min}$ for $\varepsilon < 10^{-1}$.

To corroborate the independence of the established relation between $\lambda_B^{\min}$ and $\lambda_S^{\max}$ from geometrical factors, we carry out the above analysis for a square-shaped inclusion, i.e. $\Gamma_\varepsilon = \partial(-\varepsilon, \varepsilon)^2$ in a squared domain $\Omega = (-1, 1)^2$. A comparison

[5] For each ε we consider a sequence of eigenvalues λ_{h_l} computed on meshes with sizes h_l. We terminate the sequence once the relative error between subsequent eigenvalues, $|\lambda_{h_l} - \lambda_{h_{l+1}}|/\lambda_{h_l}$, is less than 10^{-4}.

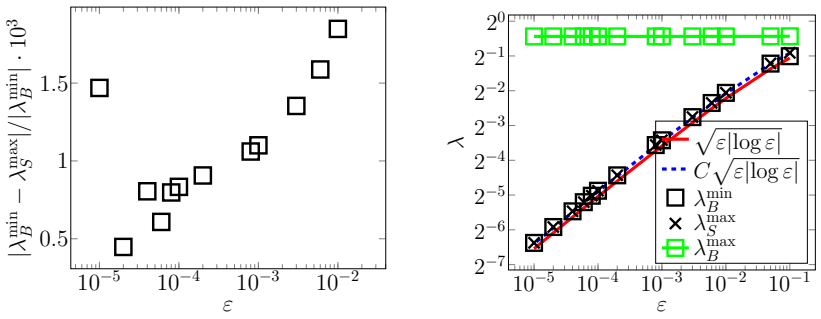

Fig. 14 (Left) Error between the smallest eigenvalue $\lambda_B^{\min}$ of the Schur complement problem (21) and the largest eigenvalue $\lambda_S^{\max}$ of the Steklov problem (23) on squared domain $\Omega = (-1, 1)^2$. In both cases, values from the finest level of refinement are considered, i.e. $\lambda_X := \lambda_{X,h_{\min}}$. (Right) Dependence of the Schur complement eigenvalues on the radius of coupling curve $\Gamma_\varepsilon = \partial(-\varepsilon, \varepsilon)^2$. Value $C \approx 1.116$ is obtained by fitting values $\lambda_B^{\min}$ for $\varepsilon < 10^{-1}$.

between the obtained values of $\lambda_S^{\max}(\varepsilon)$ and $\lambda_B^{\min}(\varepsilon)$, is depicted in Figure 14 (see also the Appendix for additional results). No significant differences are reported. The relative error between the eigenvalues remains well below the percentage point, and the expression $C\sqrt{\varepsilon|\log\varepsilon|}$ retraces $\lambda_B^{\min}(\varepsilon)$ with a constant $C \approx 1.116$.

Having shown independence of our observations from the shape of the inclusion/coupling surface, the effect of the meshing strategy and the discretization of finite elements will be investigated using a circular embedded domain Γ_ε. To exclude any relevant influence of the mesh on the obtained results, the same analysis has been repeated on a specific type of mesh, which we shall refer to as *layered*, and which has the peculiarity of being Γ_{ε_i}-conformal (Ω vertices and edges are consistent with Γ_{ε_i} ones) for every value of $\varepsilon_i \in I$ simultaneously; cf. Figure 15. In such a way, the

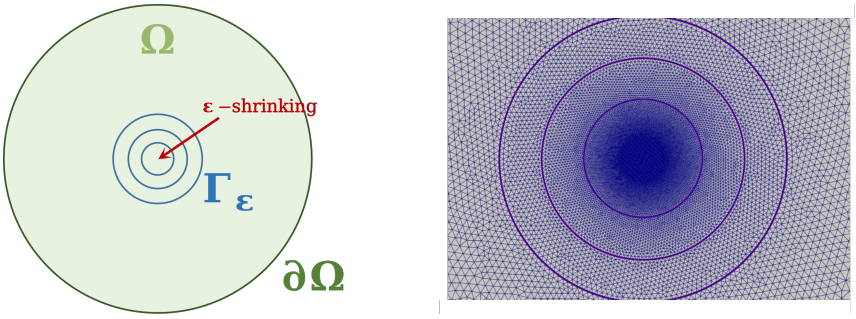

Fig. 15 (Left) Pictorial representation of the inner-radius shrinking process. (Right) Partial representation (zoomed toward the Ω center) of the *layered* mesh. The mesh has the property of being simultaneously conforming to every Γ_{ε_i}, $\varepsilon_i \in I$ (purple circles).

mesh configuration, which is the same for every value of the inner radius, cannot be held responsible for any effects on λ-ε relations. The results are plotted in Figure 16

(left). The relative difference between the values of $\lambda_B^{\max}(\varepsilon)$, $\lambda_B^{\min}(\varepsilon)$ and $\lambda_S^{\max}(\varepsilon)$ obtained on different meshes (each conformal to a specific Γ_{ε_i}) and those obtained on the layered mesh differs by less than one percentage point. Consequently, the same relation as plotted in Figure 13 between $\lambda_S^{\max}(\varepsilon)$ and $\lambda_B^{\min}(\varepsilon)$ also holds for the values obtained on the layered mesh. In conclusion, the results do not undergo significant grid influence. Additional numerical results in support of this conclusion can be found in Appendix.

In addition to the geometrical factors (shape, mesh), our aim is to exclude possible effects of different polynomial order between the spaces $2d$ and $1d$. The results of the comparison between the discretization $\mathbb{P}_1 - \mathbb{P}_1$ and $\mathbb{P}_2 - \mathbb{P}_1$ (continuous elements $\mathbb{P}_2$ for Ω and $\mathbb{P}_1$ for Γ_{ε_i}) are plotted in Figure 16. No noticeable difference can be attributed to the change of polynomial order, except for the effects on $\lambda_B^{\max}(\varepsilon)$, which differ more than 1%, but still remain independent of ε_i. From this, we can deduce that also for the $\mathbb{P}_2 - \mathbb{P}_1$ discretization, $\lambda_B^{\min} \approx \lambda_S^{\max} \sim \sqrt{\varepsilon|\log\varepsilon|}$. Thus, no relevant role of the polynomial degree on the results can be experienced (for detailed results see the Appendix).

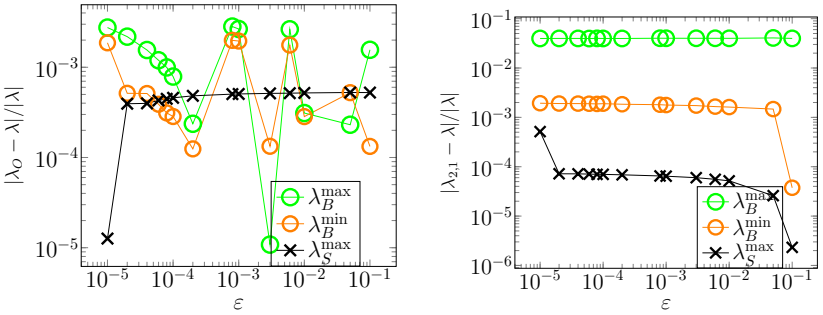

Fig. 16 Relative error $|\lambda_* - \lambda|/|\lambda|$, where λ spans $\{\lambda_B^{\max}, \lambda_B^{\min}, \lambda_S^{\max}\}$ eigenvalues obtained with standard meshing procedure (each grid conforming to a specific Γ_{ε_i}; see Figure 13). (Left) $\lambda_* \equiv \lambda_O$ spans $\{\lambda_{B,O}^{\max}, \lambda_{B,O}^{\min}, \lambda_{S,O}^{\max}\}$ obtained on the *layered* mesh in Figure 15 and denoted by the subscript "O". (right) $\lambda_* \equiv \lambda_{2,1}$ spans $\{\lambda_{B,2,1}^{\max}, \lambda_{B,2,1}^{\min}, \lambda_{S,2,1}^{\max}\}$ obtained with a $\mathbb{P}_2 - \mathbb{P}_1$ discretization and denoted by subscript "2, 1".

4.3 The $2d$-$0d$ formulation for the perforated domain problem

The link between stability of (15) and inner radius ε via the constant of the inverse trace inequality, which we demonstrated above for $2d$-$1d$ trace problem, naturally extends to $3d$-$2d$ coupling as well. In connection with the $3d$-$1d$ problem (6) we may ask if the dimensional reduction removes the observed effect of ε. To address this question we continue our investigations by applying model reduction to (15) leading (formally) to the system

$$\begin{aligned} -\Delta u &= 0 && \text{in } \Omega \subset \mathbb{R}^2, \\ \bar{u} &= g && \text{on } \Gamma, \\ u &= 0 && \text{on } \partial\Omega. \end{aligned} \tag{24}$$

We recall that $\bar{u}$ computes a mean of function $u : \Omega \to \mathbb{R}$ over the curve $\Gamma = \Gamma_\varepsilon$, i.e. $\bar{u} = |\Gamma|^{-1} \int_\Gamma u$. Note that through u and $\bar{u}$ the coupled problem (24) includes a dimensional gap of 2 (as in the case of the $3d$-$1d$ problem (6)).

Letting $V = H^1_0(\Omega)$ and $Q = \mathbb{R}$ the weak form of (24) read: Find $u \in V$, $p_\odot \in Q$ such that

$$\begin{aligned} \int_\Omega \nabla u \cdot \nabla v - \int_\Gamma p_\odot \bar{v} = 0 \quad \forall v \in V, \\ - \int_\Gamma q_\odot \bar{u} = 0 \quad \forall q_\odot \in Q. \end{aligned} \tag{25}$$

For well-posedness of (25) when $\Gamma \subset \partial\Omega$ we refer to [15]. Here we shall consider Q with an inner product $(p_\odot, q_\odot)_Q = \int_\Gamma p_\odot q_\odot$ inducing the norm $\|p_\odot\|_Q = (p_\odot, p_\odot)_Q^{1/2}$. On V, the norm is given by the H^1-seminorm. From the point of Brezzi theory, a convenient property of the reduced problem is the fact that Q is one-dimensional. Thus, the Schur complement spectrum (21) contains only a single eigenvalue λ_B. Then, Figure 17 shows computational evidence for the stability of (25) in $V \times Q$ with the chosen norms. Specifically, taking $\Omega = \{x \in \mathbb{R}^2 : |x| < 1\}$ such that the triangulation of the domain always conforms to Γ_ε, and using $\mathbb{P}_1$ elements, it can be seen that the Brezzi constant(s) related to the coupling operator[6] are bounded in the mesh size. However, similar to the full problem (15) we observe that the numerical inf-sup/B-boundedness constant λ_B decreases with radius ε, that is, $\lambda_B = \lambda_B(\varepsilon)$.

As with the $2d$-$1d$ problem, we claim that λ_B is closely linked to a Steklov eigenvalue. In this case, we consider: Find $u \in V$, $\lambda_S > 0$ satisfying

$$\int_\Gamma \bar{u}\bar{v} = \lambda_S^2 \int_\Omega \nabla u \cdot \nabla v \quad \forall v \in V. \tag{26}$$

From (26) it follows that the maximal eigenvalue λ_S relates to the estimates of the mean value of u in Γ_ε, that is,

$$\|\bar{u}\|_Q \leq \lambda_S \|u\|_V \quad \forall u \in V.$$

The relation between the two eigenvalues is demonstrated in Figure 17 which shows the relative error between the eigenvalues λ_B of the Schur complement of (25) and λ_S. Here, only the values obtained on the finest meshes for each ε are considered, that is, $\lambda_S = \lambda_{S,h_{\min}}$ and analogously for λ_B. In all cases, the observed error is $\sim 10^{-3}$.

Finally, in Figure 18 we measure the dependence of λ_S (and λ_B) on the radius ε. It can be seen that the relation is practically identical to that of the unreduced $2d$-$1d$

[6] The Brezzi conditions for the bilinear form a stemming from (25) are easily verified and the related constants take the value 1.

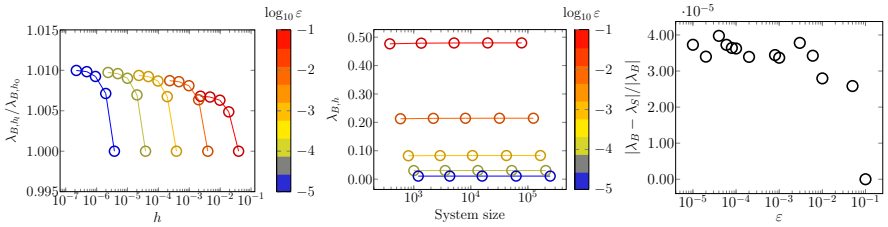

Fig. 17 (Left, center) Mesh convergence of the Schur complement eigenvalue of (25) for $\Omega = \{x \in \mathbb{R}^2,\ |x| < 1\}$, $\Gamma_\varepsilon = \{x \in \Omega,\ |x| = \epsilon\}$ and $\mathbb{P}_1$. For each ε a sequence of problems is considered in uniformly refined meshes starting from size $h_0 \geq h_l \geq h_{\min}$ leading to eigenvalues λ_{B,h_l}. (Right) Error between the Schur complement eigenvalues and the eigenvalues of the Steklov problem (26). In both cases, results for $h_l = h_{\min}$ are shown.

problem (15), see also [24]. In particular, λ_B goes to 0 together with ε, and the affect of the inner radius on stability is not removed by model reduction.

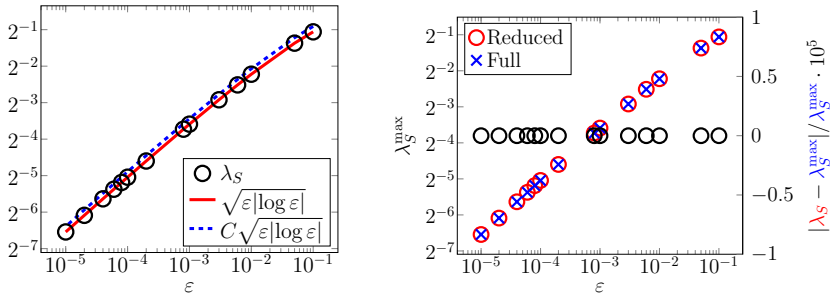

Fig. 18 (Left) Dependence of the Steklov eigenvalue $\lambda_{S,h_{\min}}$ (black $\circ$ markers) in (26) on the radius of coupling curve $\Gamma_\varepsilon = \{x \in \Omega, |x| = \epsilon\}$. The constant $C \approx 0.999$ was optimized for the best fit of the data. (Right) Comparison of the largest eigenvalues of the Steklov problems. The $2d$-$1d$ problem (16) is related to (23) with eigenvalues $\lambda_S^{\max} = \lambda_{S,h_{\min}}^{\max}$ (blue $\times$ markers), cf. Figure 13, while λ_S (red $\circ$ markers) denotes eigenvalues of (26) related to $2d$-$0d$ problem (25), see Figure 17. The relative error between the values of the full and reduced models is plotted against the right vertical axis in black markers $\circ$.

In summary, we have established, through both numerical experiments and analytical expressions about the inf-sup and trace constant, a clear relationship between β and ε

$$\beta = C\sqrt{\varepsilon|\log\varepsilon|} \quad \text{as} \quad \varepsilon \to 0 \tag{27}$$

with C a constant independent from ε. The result appears independent from the discretization parameters of the considered numerical framework, so that we can assert with reasonable confidence that such behavior is inherent in the trace/extension operator structure of the interface problem.

5 Conclusion

The solvability of mixed-dimensional problems plays a crucial role in effectively applying these models to real-world scenarios, such as microcirculation. In our research, we have focused on operator preconditioning as a means to address this issue. We have shown that by employing suitable weighted norms, the operator preconditioning framework can successfully handle material parameters such as diffusivity in both the $3d$ and $1d$ domains. However, when dealing with interface-coupled systems, these norms alone are insufficient to ensure robustness regarding geometric parameters, such as the inner radius. Through extensive numerical experiments, we have highlighted the significant impact of the parameter ε on the mathematical structure of the problem and its adverse effect on the well-posedness through the trace operator. It is worth noting that this behavior persists even in a non-topologically reduced framework. Therefore, the reduction of dimensionality and the use of appropriately scaled Sobolev spaces currently do not guarantee the robustness of preconditioners as ε approaches zero. In our view, these findings strongly advocate a thorough and fundamental analysis of the trace operator's role in coupling conditions within mixed-dimensional approaches. The ultimate goal is to develop a generalized trace operator capable of facilitating a robust coupling of partial differential equations across high-dimensional gaps.

Acknowledgement

Paolo Zunino acknowledges the support of the grant MUR PRIN 2022 No. 2022WKWZA8 *Immersed methods for multiscale and multiphysics problems* (IMMEDIATE). The present research is part of the activities of the Dipartimento di Eccellenza 2023-2027 project, funded by MUR. Nunzio Dimola and Paolo Zunino are members of the Gruppo Nazionale per il Calcolo Scientifico (GNCS), Istituto Nazionale di Alta Matematica (INdAM).

References

1. Arnold, D.N., Rognes, M.E.: Stability of Lagrange elements for the mixed Laplacian. Calcolo **46**(4), 245–260 (2009)
2. Bærland, T., Kuchta, M., Mardal, K.A.: Multigrid methods for discrete fractional sobolev spaces. SIAM Journal on Scientific Computing **41**(2), A948–A972 (2019). DOI 10.1137/18M1191488
3. Blake, T., Gross, J.: Analysis of coupled intra- and extraluminal flows for single and multiple capillaries. Mathematical Biosciences **59**(2), 173–206 (1982)
4. Braess, D.: Stability of saddle point problems with penalty. ESAIM: Mathematical Modelling and Numerical Analysis-Modélisation Mathématique et Analyse Numérique **30**(6), 731–742 (1996)

5. Bramble, J.H., Pasciak, J.E., Vassilevski, P.S.: Computational scales of Sobolev norms with application to preconditioning. Math. Comp. **69**(230), 463–480 (2000). DOI 10.1090/S0025-5718-99-01106-0
6. Brezzi, F.: On the existence, uniqueness and approximation of saddle-point problems arising from Lagrangian multipliers. Publications mathématiques et informatique de Rennes (S4), 1–26 (1974)
7. Budiša, A., Hu, X., Kuchta, M., Mardal, K.A., Zikatanov, L.: Rational approximation preconditioners for multiphysics problems. In: International Conference on Numerical Methods and Applications, pp. 100–113. Springer (2022)
8. Budiša, A., Hu, X., Kuchta, M., Mardal, K.A., Zikatanov, L.: Rational approximation preconditioners for multiphysics problems. In: I. Georgiev, M. Datcheva, K. Georgiev, G. Nikolov (eds.) Numerical Methods and Applications, pp. 100–113. Springer Nature Switzerland, Cham (2023)
9. Cerroni, D., Laurino, F., Zunino, P.: Mathematical analysis, finite element approximation and numerical solvers for the interaction of 3d reservoirs with 1d wells. GEM-International Journal on Geomathematics **10**, 1–27 (2019)
10. D'Angelo, C.: Multi scale modelling of metabolism and transport phenomena in living tissues, PhD Thesis. EPFL, Lausanne (2007)
11. D'Angelo, C.: Finite element approximation of elliptic problems with Dirac measure terms in weighted spaces: applications to one-and three-dimensional coupled problems. SIAM Journal on Numerical Analysis **50**(1), 194–215 (2012)
12. D'Angelo, C., Quarteroni, A.: On the coupling of 1d and 3d diffusion-reaction equations: Application to tissue perfusion problems. Mathematical Models and Methods in Applied Sciences **18**(08), 1481–1504 (2008)
13. Fleischman, G., Secomb, T., Gross, J.: The interaction of extravascular pressure fields and fluid exchange in capillary networks. Mathematical Biosciences **82**(2), 141–151 (1986)
14. Flieschman, G., Secomb, T., Gross, J.: Effect of extravascular pressure gradients on capillary fluid exchange. Mathematical Biosciences **81**(2), 145–164 (1986)
15. Formaggia, L., Vergara, C.: Defective Boundary Conditions for PDEs with Applications in Haemodynamics, pp. 285–312. Springer International Publishing, Cham (2018)
16. Führer, T.: Multilevel decompositions and norms for negative order Sobolev spaces. Math. Comp. **91**(333), 183–218 (2021). DOI 10.1090/mcom/3674
17. Gjerde, I.G., Kumar, K., Nordbotten, J.M.: A singularity removal method for coupled 1D–3D flow models. Computational Geosciences pp. 1–15 (2019)
18. Gregorio, S.d., Possenti, L., di Gregorio, S., Gerosa, F.M., Raimondi, G., Casagrande, G., Costantino, M.L., Zunino, P.: A computational model for microcirculation including fahraeus-lindqvist effect, plasma skimming and fluid exchange with the tissue interstitium. International Journal for Numerical Methods in Biomedical Engineering **0**(ja)
19. Hartung, G., Badr, S., Moeini, M., Lesage, F., Kleinfeld, D., Alaraj, A., Linninger, A.: Voxelized simulation of cerebral oxygen perfusion elucidates hypoxia in aged mouse cortex. PLOS Computational Biology **17**(1), 1–28 (2021). URL https://doi.org/10.1371/journal.pcbi.1008584
20. Hersch, J., Payne, L.E., Schiffer, M.M.: Some inequalities for Stekloff eigenvalues. Archive for Rational Mechanics and Analysis **57**(2), 99–114 (1974)
21. Hu, X., Keilegavlen, E., Nordbotten, J.M.: Effective preconditioners for mixed-dimensional scalar elliptic problems. Water Resources Research **59**(1), e2022WR032985 (2023)
22. Koch, T., Heck, K., Schröder, N., Class, H., Helmig, R.: A new simulation framework for soil–root interaction, evaporation, root growth, and solute transport. Vadose Zone Journal **17**(1) (2018)
23. Koch, T., Schneider, M., Helmig, R., Jenny, P.: Modeling tissue perfusion in terms of 1d-3d embedded mixed-dimension coupled problems with distributed sources. Journal of Computational Physics **410**, 109370 (2020)
24. Köppl, T., Vidotto, E., Wohlmuth, B., Zunino, P.: Mathematical modeling, analysis and numerical approximation of second-order elliptic problems with inclusions. Mathematical Models and Methods in Applied Sciences **28**(05), 953–978 (2018)

25. Köppl, T., Wohlmuth, B.: Optimal a priori error estimates for an elliptic problem with Dirac right-hand side. SIAM Journal on Numerical Analysis **52**(4), 1753–1769 (2014)
26. Kuchta, M.: Assembly of multiscale linear PDE operators. In: Numerical Mathematics and Advanced Applications ENUMATH 2019, pp. 641–650. Springer (2021)
27. Kuchta, M., Laurino, F., Mardal, K.A., Zunino, P.: Analysis and approximation of mixed-dimensional PDEs on 3D-1D domains coupled with Lagrange multipliers. SIAM Journal on Numerical Analysis **59**(1), 558–582 (2021)
28. Kuchta, M., Mardal, K.A., Mortensen, M.: Preconditioning trace coupled 3d-1d systems using fractional Laplacian. Numerical Methods for Partial Differential Equations **0**(0)
29. Kuchta, M., Nordaas, M., Verschaeve, J., Mortensen, M., Mardal, K.: Preconditioners for saddle point systems with trace constraints coupling 2d and 1d domains. SIAM Journal on Scientific Computing **38**(6), B962–B987 (2016)
30. Köppl, T., Vidotto, E., Wohlmuth, B., Zunino, P.: Mathematical modeling, analysis and numerical approximation of second-order elliptic problems with inclusions. Mathematical Models and Methods in Applied Sciences **28**(5), 953–978 (2018)
31. Laurino, F., Zunino, P.: Derivation and analysis of coupled PDEs on manifolds with high dimensionality gap arising from topological model reduction. ESAIM: M2AN **53**(6), 2047–2080 (2019)
32. Lions, J.L., Magenes, E.: Non-homogeneous boundary value problems and applications: Vol. 1, vol. 181. Springer Science & Business Media (2012)
33. Logg, A., Mardal, K.A., Wells, G.N., et al.: Automated Solution of Differential Equations by the Finite Element Method. Springer (2012)
34. Mardal, K.A., Winther, R.: Preconditioning discretizations of systems of partial differential equations. Numerical Linear Algebra with Applications **18**(1), 1–40 (2011)
35. Maury, B.: Numerical analysis of a finite element/volume penalty method. SIAM Journal on Numerical Analysis **47**(2), 1126–1148 (2009). DOI 10.1137/080712799
36. Murphy, M.F., Golub, G.H., Wathen, A.J.: A note on preconditioning for indefinite linear systems. SIAM Journal on Scientific Computing **21**(6), 1969–1972 (2000)
37. Nečas, J.: Direct methods in the theory of elliptic equations. Springer Science & Business Media (2011)
38. Nitsche, J.: Über ein variationsprinzip zur lösung von dirichlet-problemen bei verwendung von teilräumen, die keinen randbedingungen unterworfen sind. Abhandlungen aus dem Mathematischen Seminar der Universität Hamburg **36**(1), 9–15 (1971). DOI 10.1007/BF02995904
39. Peaceman, D.: Interpretation of well-block pressures in numerical reservoir simulation. Soc Pet Eng AIME J **18**(3), 183–194 (1978)
40. Peaceman, D.W.: Interpretation of well-block pressures in numerical reservoir simulation with nonsquare grid blocks and anisotropic permeability. Society of Petroleum Engineers journal **23**(3), 531–543 (1983)
41. Qin, J.: On the convergence of some low order mixed finite elements for incompressible fluids. The Pennsylvania State University (1994)
42. Rognes, M.E.: Automated testing of saddle point stability conditions. In: Automated Solution of Differential Equations by the Finite Element Method: The FEniCS Book, pp. 657–671. Springer (2012)
43. Rusten, T., Winther, R.: A preconditioned iterative method for saddlepoint problems. SIAM Journal on Matrix Analysis and Applications **13**(3), 887–904 (1992)
44. Saad, Y.: Iterative methods for sparse linear systems. SIAM (2003)
45. Secomb, T., Hsu, R., Park, E., Dewhirst, M.: Green's function methods for analysis of oxygen delivery to tissue by microvascular networks. Annals of Biomedical Engineering **32**(11), 1519–1529 (2004)
46. Steinbach, O.: Numerical approximation methods for elliptic boundary value problems: finite and boundary elements. Springer Science & Business Media (2007)
47. Ventimiglia, T., Linninger, A.A.: Mesh-free high-resolution simulation of cerebrocortical oxygen supply with fast fourier preconditioning. International Journal for Numerical Methods in Biomedical Engineering **39**(8), e3735 (2023). DOI https://doi.org/10.1002/cnm.3735

6 Appendix

6.1 Numerical experiments for square-shaped inclusion

For the sake of comparison of the effect of the inclusion shape on the relation between the well-posedness of (16) and the diameter of the inclusion, we collect here additional results for $\Gamma_\varepsilon = \partial(-\varepsilon,\varepsilon)^2$ and $\Omega = (-1,1)^2$. These results are analogous to Figure 12 and Figure 18 where circular Γ_ε is considered.

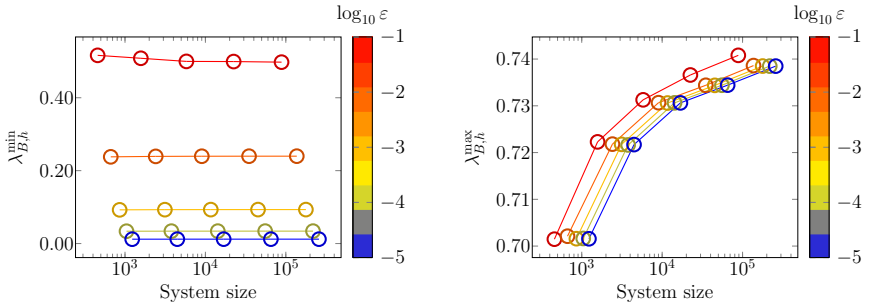

Fig. 19 (Left) Mesh convergence of the extremal eigenvalues of Schur complement (21) for $\Omega = (-1,1)^2$, $\Gamma_\varepsilon = \partial(-\varepsilon,\varepsilon)^2$. Both spaces V and Q are discretized by $\mathbb{P}_1$ elements. For each ε a sequence of problems is considered on uniformly refined meshes starting from size $h_0 \geq h_l \geq h_{\min}$ leading to eigenvalues λ_{B,h_l}.

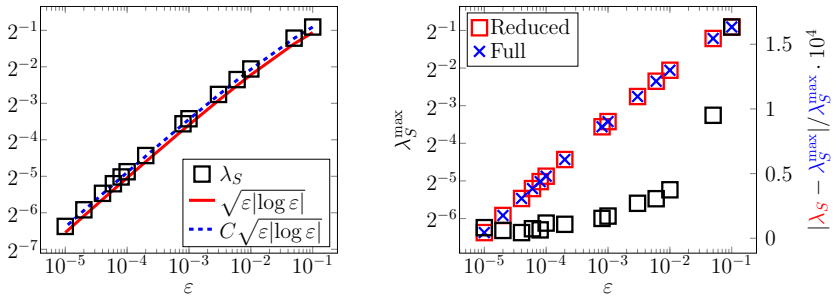

Fig. 20 Dependence of the Steklov eigenvalue $\lambda_{S,h_{\min}}$ in (26) on the radius of coupling curve $\Gamma_\varepsilon = \partial(-\varepsilon,\varepsilon)^2$. The constant $C \approx 1.116$ was optimized for the best fit of the data. (Right) Comparison of the largest eigenvalues of the Steklov problems. The $2d$-$1d$ problem (16) is related to (23) with eigenvalues $\lambda^{\max} = \lambda^{\max}_{S,h_{\min}}$, cf. Figure 13, while λ_S denotes eigenvalues of (26) related to $2d$-$0d$ problem (25), see Figure 17. The relative error between the values of the full and reduced models is plotted against the right vertical axis in black markers □.

6.2 Numerical experiments for layered mesh

Here we collect additional results regarding the numerical experiments for a circular domain $\Omega = \{x \in \mathbb{R}^2, |x| < 1\}$ with circular inclusion $\Gamma_\varepsilon = \{x \in \Omega, |x| = \varepsilon\}$ obtained on layered mesh (see Figure 15 (right)) conformal simultaneously to every Γ_{ε_i}, with $\varepsilon_i \in \{10^{-1}, 10^{-2}, 10^{-3}, 10^{-4}, 10^{-5}\}$.

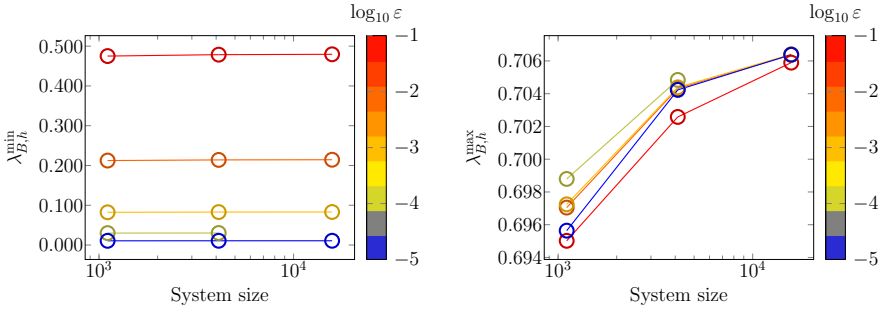

Fig. 21 (Left) Mesh convergence of the extremal eigenvalues of Schur complement (21) for $\Omega = \{x \in \mathbb{R}^2, |x| < 1\}, \Gamma_\varepsilon = \{x \in \Omega, |x| = \varepsilon\}$. Both spaces V and Q are discretized by $\mathbb{P}_1$ elements. For each ε a sequence of problems is considered on a uniformly refined layered mesh starting from size $h_0 \geq h_l \geq h_{\min}$ leading to eigenvalues λ_{B,h_l}.

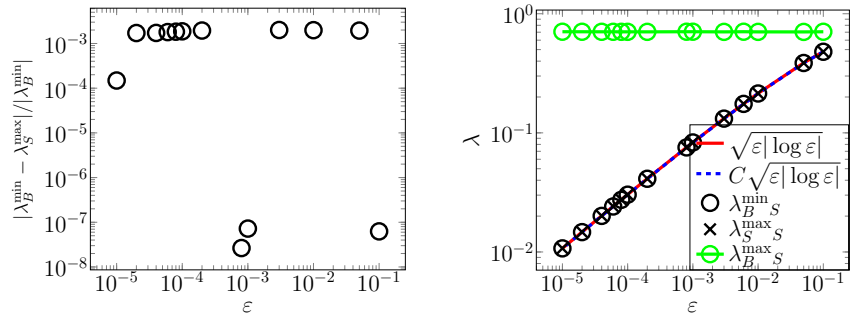

Fig. 22 Error between the smallest eigenvalue $\lambda^{\min}_B$ of the Schur complement problem (21) and the largest eigenvalue $\lambda^{\max}_S$ of the Steklov problem (23). In both cases, values of the finest level of refinement are considered, that is, $\lambda_X := \lambda_{X,h_{\min}}$. (Right) Dependence of the eigenvalues of the radius of the coupling curve $\Gamma_\varepsilon = \{x \in \Omega, |x| = \varepsilon\}$. The value $C \approx 0.999$ is obtained by fitting values $\lambda^{\min}_B$ for $\varepsilon < 10^{-1}$.

6.3 Numerical experiments for $\mathbb{P}_2 - \mathbb{P}_1$ discretization

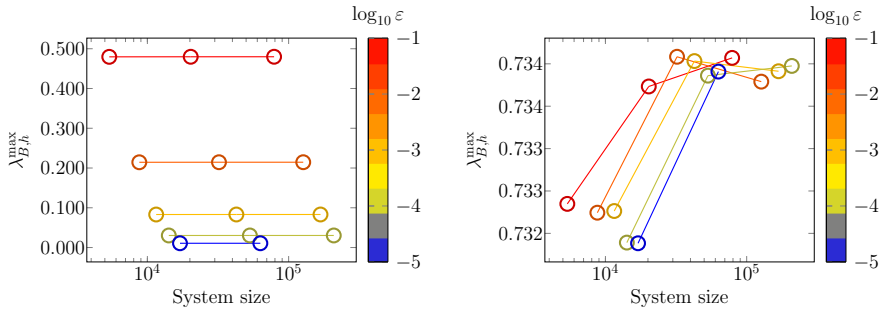

Fig. 23 (Left) Mesh convergence of the extremal eigenvalues of Schur complement (21) for $\Omega = \{x \in \mathbb{R}^2,\ |x| < 1\}$, $\Gamma_\varepsilon = \{x \in \Omega,\ |x| = \varepsilon\}$. Spaces V and Q are discretized respectively by $\mathbb{P}_2$ and $\mathbb{P}_1$ elements. For each ε a sequence of problems is considered on uniformly refined meshes starting from size $h_0 \geq h_l \geq h_{\min}$ leading to eigenvalues λ_{B,h_l}.

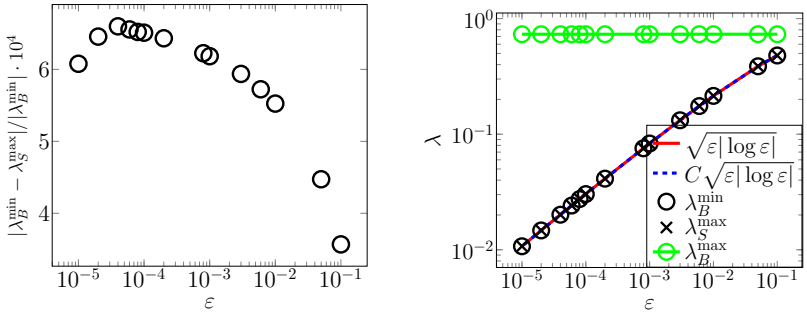

Fig. 24 Error between the smallest eigenvalue $\lambda_B^{\min}$ of the Schur complement problem (21) and the largest eigenvalue $\lambda_S^{\max}$ of the Steklov problem (23). In both cases, values of the finest level of refinement are considered, that is, $\lambda_X := \lambda_{X,h_{\min}}$. (Right) Dependence of the eigenvalues of the radius of the coupling curve $\Gamma_\varepsilon = \{x \in \Omega, |x| = \varepsilon\}$. The value $C \approx 0.999$ is obtained by fitting values $\lambda_B^{\min}$ for $\varepsilon < 10^{-1}$.

MOX Technical Reports, last issues

Dipartimento di Matematica
Politecnico di Milano, Via Bonardi 9 - 20133 Milano (Italy)

102/2023 Dimola N.; Kuchta M.; Mardal K.A.; Zunino P.
Robust Preconditioning of Mixed-Dimensional PDEs on 3d-1d domains coupled with Lagrange Multipliers

101/2023 Formaggia, L.; Zunino, P.
Hybrid dimensional models for blood flow and mass transport

98/2023 Lespagnol, F.; Grandmont, C.; Zunino, P.; Fernandez, M.A.
A mixed-dimensional formulation for the simulation of slender structures immersed in an incompressible flow

100/2023 Vitullo, P.; Cicci, L.; Possenti, L.; Coclite, A.; Costantino, M.L.; Zunino, P.
Sensitivity analysis of a multi-physics model for the vascular microenvironment

96/2023 Bonetti, S.; Botti, M.; Antonietti, P.F.
Robust discontinuous Galerkin-based scheme for the fully-coupled non-linear thermo-hydro-mechanical problem

95/2023 Barnafi, N. A.; Regazzoni, F.; Riccobelli, D.
Reconstructing relaxed configurations in elastic bodies: mathematical formulation and numerical methods for cardiac modeling

93/2023 Andrini, D.; Magri, M.; Ciarletta, P.
Optimal surface clothing with elastic nets

92/2023 Burzacchi, A.; Rossi, L.; Agasisti, T.; Paganoni, A. M.; Vantini, S.
Commuting time as a determinant of higher education students' performance: the case of Politecnico di Milano

Burzacchi, A.; Rossi, L.; Agasisti, T.; Paganoni, A. M.; Vantini, S.
Commuting time as a determinant of higher education students' performance: the case of Politecnico di Milano

90/2023 Gregorio, C.; Baj, G.; Barbati, G.; Ieva, F.
Dynamic treatment effect phenotyping through functional survival analysis